AALTO UNIVERSITY
SCHOOL OF ELECTRICAL ENGINEERING

Department of Electrical Engineering

Sabin Sathyan

Synchronous Reluctance Motor for Household Applications

Thesis submitted for examination for the degree of Master of Science in Technology.

Espoo

Thesis Supervisor:

Professor Antero Arkkio

AALTO UNIVERSITY

SCHOOL OF ELECTRICAL ENGINEERING Abstract of the Master's Thesis

Author: Sabin Sathyan

Name of the thesis: Synchronous Reluctance Motor for Household Applications

Date: 12.03.2013 Language: English Number of pages: xi+45

Department of Electrical Engineering

Professorship: Electromechanics Code: S-17

Supervisor and Instructor: Prof. Antero Arkkio

Abstract

This thesis has been done in the Electromechanics group of Department of Electrical Engineering, Aalto University as part of the motor design and electromechanics research. The project is centered on the design of synchronous reluctance motors and study on how this motor can be used for household applications. The design and simulation were carried out by using extensive finite element analysis with FCSMEK developed in the Helsinki University of Technology. The purpose was to create a motor with cheaper cost and having good performance parameters.

The main concentration in the work was on the design part, especially the rotor design, as minute design elements have considerable effect on the performance of the motor. The optimization process of the rotor design has given results on the effect of some geometrical parameters in the motor design technology. A 300 W motor is designed and a thermal model was prepared using Lumped Thermal Networking method. The motor has good efficiency and low losses with good torque characteristics. A study on the comparison of the synchronous reluctance motor with induction motor has been done in order to justify the performance of the motor and the feasibility of using this type of motor for household applications.

Keywords: Electrical Machines, Synchronous Reluctance Motor, Saliency Ratio, flux barrier, FEM (Finite Element Analysis), Thermal Modelling

Preface

This thesis was carried out during the period of June 2012 to December 2012. I would like to express my sincere gratitude to Prof. Antero Arkkio, the supervisor of my project for giving such an opportunity to do the thesis and for the valuable assistance and guidance he has given during the period of the project.

I appreciate the support and encouragement of Prof. Asko Niemenmaa and Anouar Belachen during my research. I would like to thank the operations engineer Mr. Ari Havisto for the technical assistance given and for helping me to gain other practical resources required for the thesis work. I am thankful to my colleagues in the department Devi, Andreea, Aravind, Kiran, Jonathan, Sahas, Daniel and other researchers in the team of electromechanics. Also, I am grateful to Geethu, Robin and all other friends in the University.

I thank the Almighty for the blessings and finally I wish to thank my parents Bindu and Sathyan and my brother Bibin for their love and support throughout my studies.

Espoo, March 12, 2013

Sabin Sathyan

Contents

List of Figures

List of Symbols and Abbreviations

α	Current phase
ε	Surface emissivity
η_{fin}	Number of fins
θ_p	Pole arc in radians
λ	Thermal conductivity
λ_{ds}	d axis flux linkage
λ_{qs}	q axis flux linkage
λ_s	Equivalent slot thermal conductivity
λ_{sh}	Thermal conductivity of the shaft
σ	Stefan-Boltzmann constant
τ_p	Pole pitch
ψ	Angle of the cylindrical sector
ω	Angular velocity
A_f	Cross sectional area of frame
A_r	Cross sectional area of ribs
a_r	Thickness of frame rib
a_{so}	Slot opening width
a_{st}	The width of stator tooth
b_{fin}	Width of the rotor fin
b_r	Height of frame rib
D_s	Diameter of shaft
D_{so}	Outer diameter of stator yoke

d_A	Equivalent height of the air between the insulation and teeth
d_I	Length of the slot insulation
h	Heat transfer coefficient in $W/m^2.K$
h_{ag}	The heat transfer coefficient between stator and rotor
h_{fin}	Height of the rotor fin
I_r	Rotor current
I_s	Stator current
i_{ds}	d axis flux current
i_{qs}	q axis flux current
K_w	Ratio of Insulation or flux barrier to iron rib width
k	Stacking factor
L_1	Length of rib over endcap air
L_{act}	Actual length of the motor
L_{fe}	Effective length of stator core
L_{ds}	d axis flux inductance
L_{qs}	q axis flux inductance
L_m	Induction motor magnetizing inductance
L_r	Induction motor total rotor inductance
l_{av}	Half of the average length of the coil
l_{sh}	Length of the shaft from one bearing to the other
P	Number of poles
P_{SRM}	Power loss in SRM
P_i	Power loss in Induction Motor

Q_s	Number of stator slots
q	Heat dissipation
R_a	Armature winding resistance
R_{t}	Thermal resistance of stator teeth
R_{th}	Thermal resistance
R_{yoke}	Thermal resistance of yoke
R_w	Thermal resistance of the winding
R_s	Stator resistance
R_r	Rotor resistance
r_{δ}	Average airgap length
r_s	Outer radius of stator
r_r	Outer radius of rotor
r_o	Outer radius of cylinder
r_i	Inner radius of cylinder
r_{ro}	Outer radius of rotor
r_{sh}	Outer radius of the shaft
T	Output Torque
T_{amb}	Ambient temperature
T_i	Induction motor output torque
T_s	Surface temperature
T_{SRM}	SRM output torque
V_d,	d axis component of armature voltage
V_q	q axis component of armature voltage

v_0	Velocity
W_{iron}	The width of rotor segment
W_{ins}	The flux barrier or insulation width
rpm	Revolutions per minute
SRM	Synchronous Reluctance Motor

1. Introduction

1.1 Objective

The aim of the project is to study how the Synchronous Reluctance Motor meets the requirements of the household applications. In order to study this, a 300 Watts 10000 rpm radial flux synchronous reluctance motor has to be designed. The electromagnetic characteristics are obtained from a Finite element model and the temperature rise is estimated using a thermal/network model.

1.2 Motivation behind the Project

Electric motors are used in wide range of applications in households and industries. In European Union, about 40% of the electric power produced is consumed by electric motors. In household applications, low power variable speed drives are used extensively. Most of those motors are of induction type with efficiency of 70 to 80 percentages. The efficiency level and performance can be enhanced with the use of permanent magnet motors. But, the cost of the permanent magnet materials is shooting up and hence permanent magnet motors are not an economic alternative to substitute with induction motors. At this juncture, an interest and focus on Synchronous reluctance motor (SRM) has been come up. The synchronous motor was invented in 1920s, however due to low efficiency and torque characteristics, these machines were not developed as industrial products. With the development of modern variable speed drives and power electronics converters, the operation of synchronous reluctance motors has been improved and optimized for various applications.

Synchronous Reluctance Motor has got a mounting attention in current times, as it has got low-priced construction, flux-weakening capability, high power density, “cold rotor” benefit, etc. When the application requires constant-torque performance, like the case in servo drives, Permanent Magnet synchronous motor is commonly adopted. Though high torque per volume can be obtained, the motor is quite expensive due to high cost of magnet materials. If the requirement is constant-power operation, as in the case of spindle drives, the field oriented controlled induction motor gives the requisite performance. It can be effectively used in flux-weakening, but its torque per volume is much lower than that of the PM motor. The synchronous reluctance motor is a possible solution for both of the above applications, both constant torque and constant power behaviors.

2. Synchronous Reluctance Motor

2.1 Basic Theory

The rotor of the SRM consists of direct axis where the reluctance is least and quadrature axis where the magnetic reluctance is high. When power is applied, the rotor rotates and attempts to align the magnetically conducting direction to the stator field and thus torque is produced. The figure 2.1 [16] shows the direct and quadrature axis of an SRM.

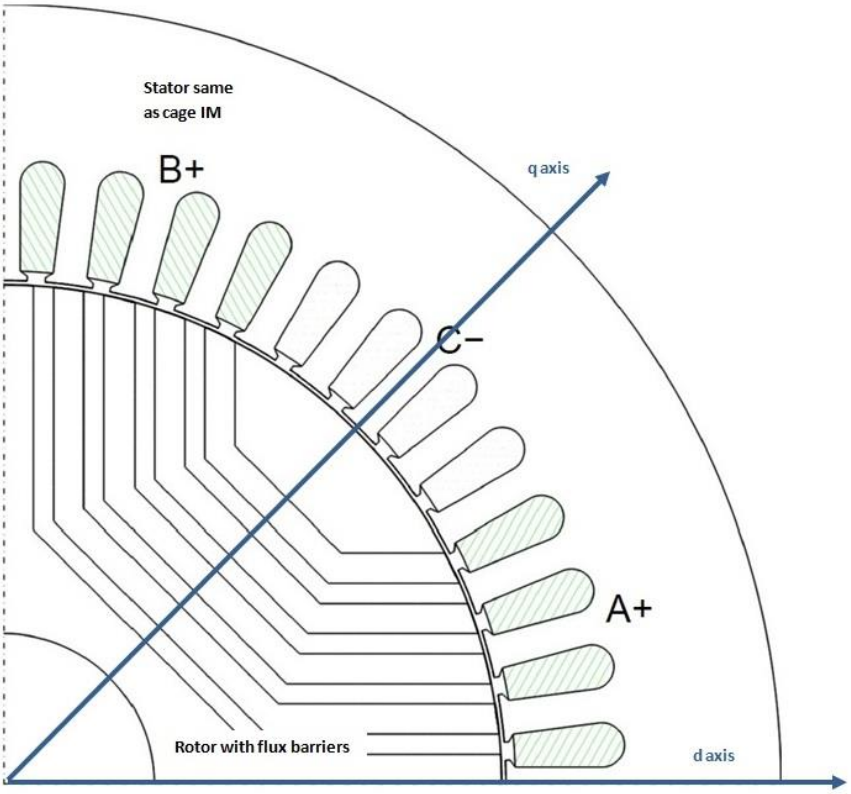

Figure 2.1 Direct and quadrature axis of the rotor

The strength of the torque produced is directly proportional to the Saliency Ratio, i.e. the ratio of direct axis inductance and quadrature axis inductance. The torque can be expressed as [8],

$$T = \frac{3}{2}\frac{P}{2}\left(\Lambda_{\mathrm{ds}} i_{\mathrm{qs}} - \Lambda_{\mathrm{qs}} i_{\mathrm{ds}}\right) \tag{2.1}$$

$\Lambda_{\mathrm{ds}}, \Lambda_{\mathrm{qs}}$ are d and q axis flux linkage

$i_{\mathrm{ds}}, i_{\mathrm{qs}}$ are d and q axis stator currents and P is the number of poles

Under normal steady state conditions, the rotor currents are zero.

$$\Lambda_{\mathrm{ds}} = L_{\mathrm{ds}} i_{\mathrm{ds}} \tag{2.2}$$

$$\Lambda_{\mathrm{qs}} = L_{\mathrm{qs}} i_{\mathrm{qs}} \tag{2.3}$$

Where L_{ds} and L_{qs} are d and q axis inductances.

Then,
$$T = \frac{3}{2}\frac{P}{2}\left(L_{\mathrm{ds}} - L_{\mathrm{qs}}\right) i_{\mathrm{ds}}\, i_{\mathrm{qs}} \tag{2.4}$$

In general, L_{ds} and L_{qs} contain both leakage and magnetizing components.

$$L_{\mathrm{ds}} = L_{\mathrm{ls}} + L_{\mathrm{md}} \tag{2.5}$$

$$L_{\mathrm{qs}} = L_{\mathrm{ls}} + L_{\mathrm{mq}} \tag{2.6}$$

Now,

$$\begin{aligned} T &= \frac{3}{2}\frac{P}{2}\left(L_{\mathrm{md}} - L_{\mathrm{mq}}\right) i_{\mathrm{ds}}\, i_{\mathrm{qs}} \\ &= \frac{3}{2}\frac{P}{2}\left(1 - \frac{L_{\mathrm{mq}}}{L_{\mathrm{md}}}\right)\left(L_{\mathrm{md}} i_{\mathrm{ds}}\right) i_{\mathrm{qs}} \end{aligned} \tag{2.7}$$

2.2 Vector Diagram

The vectors of the SRM [4] in the normal state are shown in figure 2.2

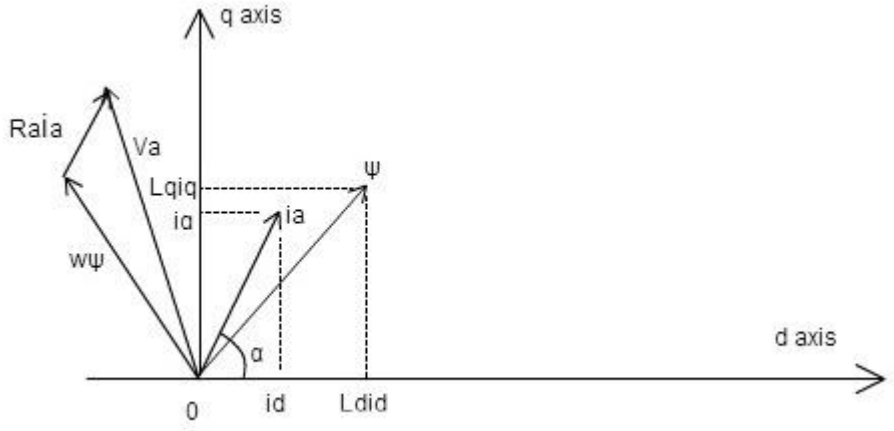

Figure 2.2 Vector diagram of SRM

$$V_{\mathrm{d}} = R_{\mathrm{a}} i_{\mathrm{d}} - \omega L_{\mathrm{q}} i_{\mathrm{q}} \tag{2.8}$$

$$V_{\mathrm{q}} = R_{\mathrm{a}} i_{\mathrm{q}} - \omega L_{\mathrm{d}} i_{\mathrm{d}} \tag{2.9}$$

$$T = P\left(L_{\mathrm{d}} - L_{\mathrm{q}}\right) i_{\mathrm{d}} i_{\mathrm{q}}$$
$$= \frac{P}{2}(L_{\mathrm{d}} - L_{\mathrm{q}}) {i^2}_{\mathrm{a}} \sin 2\alpha \qquad (2.10)$$

V_{a} – Armature voltage vector

Ψ – Interlinkage flux vector

R_{a} – Armature winding resistance

i_{a} – Armature current vector

α – Current phase

V_{d}, V_{q} – d and q axis components of armature voltage

L_{d}, L_{q} – d and q axis inductances

i_{d}, i_{q} – d and q axis currents

ω – Angular velocity

T – Torque

P – Number of poles

2.3 Equivalent Circuit

Figure 2.3 shows simple equivalent circuit of the synchronous reluctance motor [4].

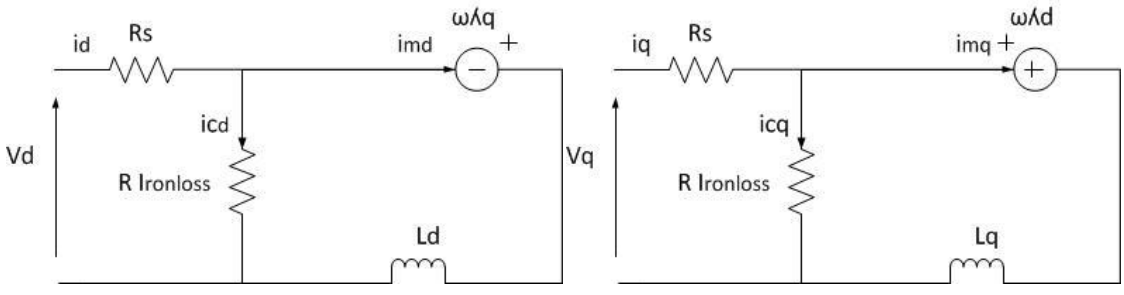

Figure 2.3 Equivalent circuits of SRM in the d and q axis reference frames

3. Comparison with Induction Motor

3.1 Torque Ratio

The induction motor torque expression is [8],

$$T_{\mathrm{i}} = \frac{3}{2}\frac{P}{2}\frac{L_{\mathrm{m}}}{L_{\mathrm{r}}}(L_{\mathrm{m}} i_{\mathrm{ds}}) i_{\mathrm{qs}} \tag{3.1}$$

Now, the performance of SRM compared to induction motor can be evaluated by taking the torque ratio,

$$\frac{T_{\mathrm{SRM}}}{T_{\mathrm{i}}} = \frac{(L_{\mathrm{md}} - L_{\mathrm{mq}})}{\frac{L_{\mathrm{m}}}{L_{\mathrm{r}}} L_{\mathrm{m}}}$$

$$= \frac{\frac{L_{\mathrm{md}}}{L_{\mathrm{m}}}\left(1 - \frac{L_{\mathrm{mq}}}{L_{\mathrm{md}}}\right)}{\frac{L_{\mathrm{m}}}{L_{\mathrm{r}}}} \tag{3.2}$$

Thus the torque ratio depends on,

- The saliency ratio $L_{\mathrm{md}}/L_{\mathrm{mq}}$
- The ratio of the SRM d-axis magnetizing inductance expressed as a fraction of the corresponding induction motor magnetizing inductance, $L_{\mathrm{md}}/L_{\mathrm{m}}$
- The induction motor magnetizing to total rotor inductance ratio $L_{\mathrm{m}}/L_{\mathrm{r}}$

Normally, the induction motor magnetizing reactance is in the range 1.0 to 2.0 per unit and the rotor leakage reactance is in the range 0.07 to 0.1. Then $L_{\mathrm{m}}/L_{\mathrm{r}}$ becomes approximately 0.95. If we consider the same air-gap length for the two machines, the ratio $L_{\mathrm{md}}/L_{\mathrm{m}}$ then depends on the width of the rotor pole or pole arc of the reluctance machine relative to the pole pitch of the stator poles of the two motors.

From [8], the relevant equation is given by,

$$\frac{L_{\mathrm{md}}}{L_{\mathrm{m}}} = \frac{\int_{\frac{\pi-\theta_{\mathrm{p}}}{2}}^{\frac{\pi+\theta_{\mathrm{p}}}{2}} \sin^2\theta \, d\theta}{\int_0^{\pi} \sin^2\theta \, d\theta} \tag{3.3}$$

$$\theta_p - \text{The pole arc in radians}$$

If we use a very conservative value of 120 degrees or (2π/3) radians,

$$\frac{L_{\mathrm{md}}}{L_{\mathrm{m}}} = \frac{\int_{\frac{\pi}{6}}^{\frac{5\pi}{6}} \sin^2\theta \, d\theta}{\int_0^{\pi} \sin^2\theta \, d\theta} \tag{3.4}$$

$$\frac{L_{\mathrm{md}}}{L_{\mathrm{m}}} = 0.94 \tag{3.5}$$

$$\text{Then, the torque ratio becomes, } \frac{T_{\mathrm{SRM}}}{T_{\mathrm{i}}} = \frac{0.94(1-\frac{1}{6})}{0.95} = 0.82 \tag{3.6}$$

3.2 Power Loss Ratio

If we consider the case of copper loss only, as the iron loss is less compared to it, the power loss in the SRM can be expressed as,

$$P_{\mathrm{SRM}} = \frac{3}{2} I^2{}_{\mathrm{s}} R_{\mathrm{s}} \tag{3.7}$$

$$\text{The induction motor losses are, } P_{\mathrm{i}} = \tfrac{3}{2}(I^2{}_{\mathrm{s}} R_{\mathrm{s}} + I^2{}_{\mathrm{r}} R_{\mathrm{r}}) \tag{3.8}$$

If the motor is loaded to run in rated current, the stator and rotor currents are nearly equal, then they can be considered as equal. Also, rotor resistance is equal to 0.75 to 1.25 times the stator resistance, and theses resistances can be considered as equal.

Now,

$$\frac{P_{\mathrm{SRM}}}{P_{\mathrm{i}}} = 0.5 \tag{3.9}$$

From the torque and power loss ratio, it can be inferred that, the synchronous reluctance motor produces about 80% of the torque that of the induction motor, while the SRM has only half of the power losses compared to the induction motor.

3.3 Motor comparison at the same power loss

From the equations 3.6 and 3.9,

Here, the following equation is obtained,

$$\frac{3}{2} I^2{}_{\mathrm{sSRM}} r_{\mathrm{sSRM}} = \frac{3}{2} (I^2{}_{si} R_{\mathrm{si}} + I^2{}_{\mathrm{ri}} R_{\mathrm{ri}}) \tag{3.10}$$

From the studies and experimental results by A.Boglietti [9], the relation between currents has been found to be,

$$I_{\mathrm{si}} = 0.78\, I_{\mathrm{sSRM}} \tag{3.11}$$

Now,

$$\frac{T_{\mathrm{SRM}}}{T_{\mathrm{i}}} = 1.19 \tag{3.12}$$

Thus, with the same dissipated power, ie. with the same stator winding temperature, synchronous reluctance motor can produce a higher torque than the induction motor.

4. Development History

4.1 Evolution of SRM Designs

The saliency ratio ξ has the major role in the performance of the motor and most of the other parameters are dependent on the same. The design ventures aiming to achieve high ξ were by providing flux guides for d axis flux to get high L_d and putting flux barriers to q axis for lowering L_q [1]. Some researchers like Miller, Cruickshank have recognized the potential of reluctance motors in their work, but due to the lack of field oriented controllers they could not achieve it in practice.

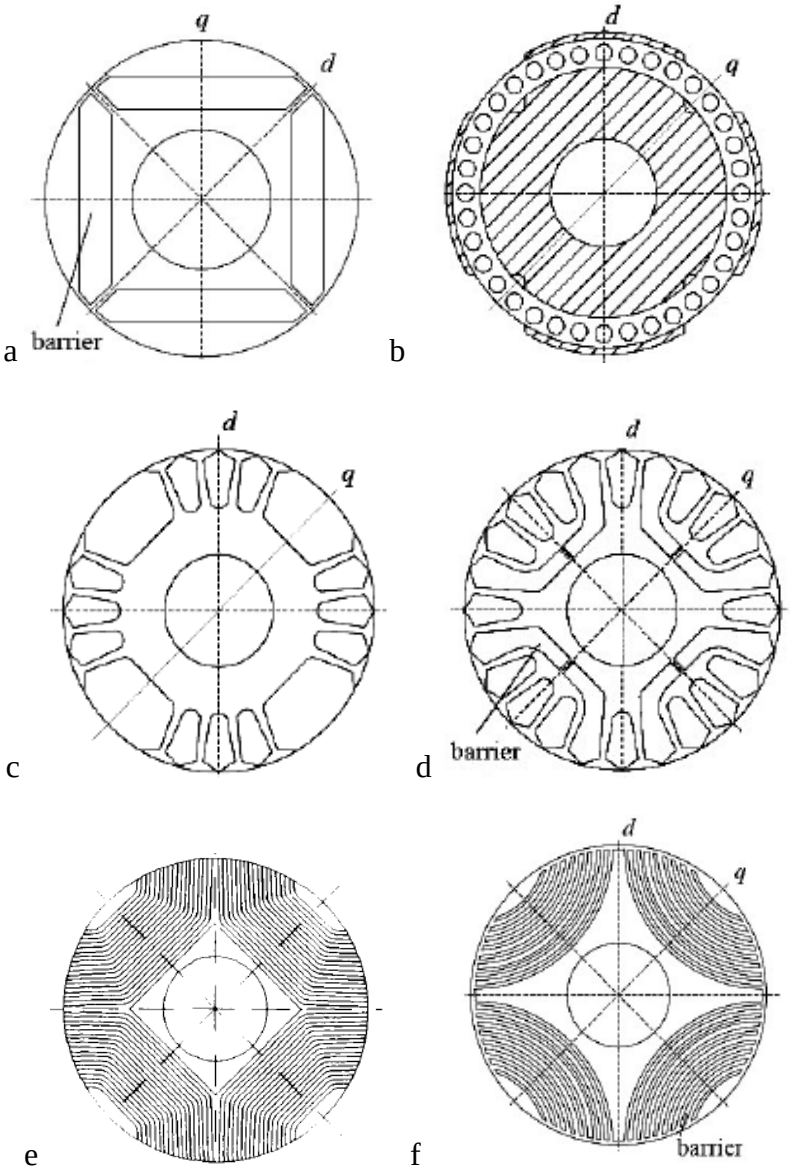

Figure 4.1 Evolution of synchronous reluctance rotor design [1]

The figure 4.1 shows the evolution of various rotor designs, in which Figs a and b represents the salient pole designs, Figs c and d show the single barrier rotor and Figs e and f are multiple barrier designs.

The salient pole type design is achieved by removal of material from a conventional induction motor, by punching before or milling after casting the cage. The saliency ratio of this kind of machine is very small and hence the performance also is poor. The second type of salient pole design like a conventional salient pole synchronous motor with windings removed, developed by Lee, Hassan and Osheiba also has not met saliency ratio more than 4.

The single barrier construction also could not achieve the required saliency ratio. In 1923, Kostko [3] has constructed a multiple barrier design as shown in Fig. e and f, in which the interpolar cutout is widened to decrease the q axis inductance, the pole arc is then narrowed and results in an unwanted reduction in L_d. Kostko analyzed that, multiple barrier design involves no sacrifice of pole arc in the d axis, and hence it is the natural way to make a synchronous reluctance motor. Researchers after Kostko, developed the geometry along two major ways, the segmental geometry as shown in Fig f and the axially laminated geometry Fig. 4.2 b, below.

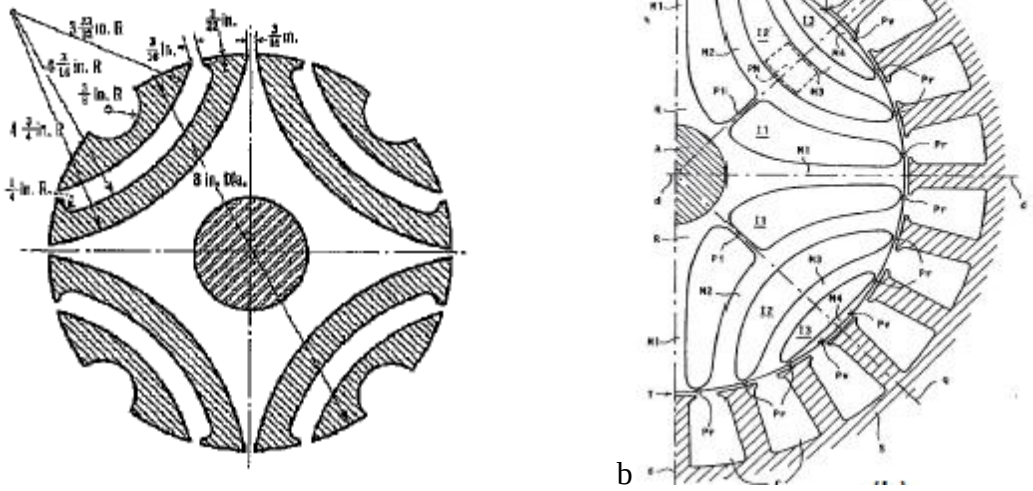

a b

Fig 4.2 First type of transversely laminated anisotropy type and its modern version [3]

5. Motor Design

5.1 Design Process

The design was done through simulations using the finite element program FCSMEK developed in the Laboratory of Electromechanics of Helsinki University of Technology. FCSMEK is a powerful program package for finite element analysis of synchronous or asynchronous radial flux machines.

The finite element analysis process is done in three stages in FCSMEK. First step is to create a finite element mesh, based on information about dimensions and parameters of the electrical machine. Second, an initial state for time-stepping analysis is solved using a DC solution. And finally, the time-stepping analysis is performed.

The objective was to develop a 300 W, 10000 rpm Synchronous reluctance motor. As far as the SRM design is considered, the design constraints are mainly the rotor parameters like the size, shape and number of flux barriers, the outer layer size, etc. Initially a plain rotor was created without any barrier and then the optimization has been done by performing extensive finite element simulation using different design parameters.

5.2 Design Parameters

5.2 a. Number of Flux barriers

The number of flux barriers has significant effect on the characteristics of SRM. During the design process, simulations have been done with different numbers of flux barriers in the rotor. It has been found out that, the output torque tends to increase with the increase in number of flux barriers. Besides, torque ripple decreased with increase in barriers. It was learned that, the increase in torque was saturated at a flux barrier number of six. Hence, in the rotor design optimization, the minimum number of flux barriers has been set as six. The Figure 5.1 shows the relation between output torque and number of flux barriers.

The q axis inductance L_q decreases up until four layers while the d axis inductance L_d increases till six layers and as a result the difference L_d-L_q which affects the torque has the same value for six layers and more. This is shown in Figure 5.1.

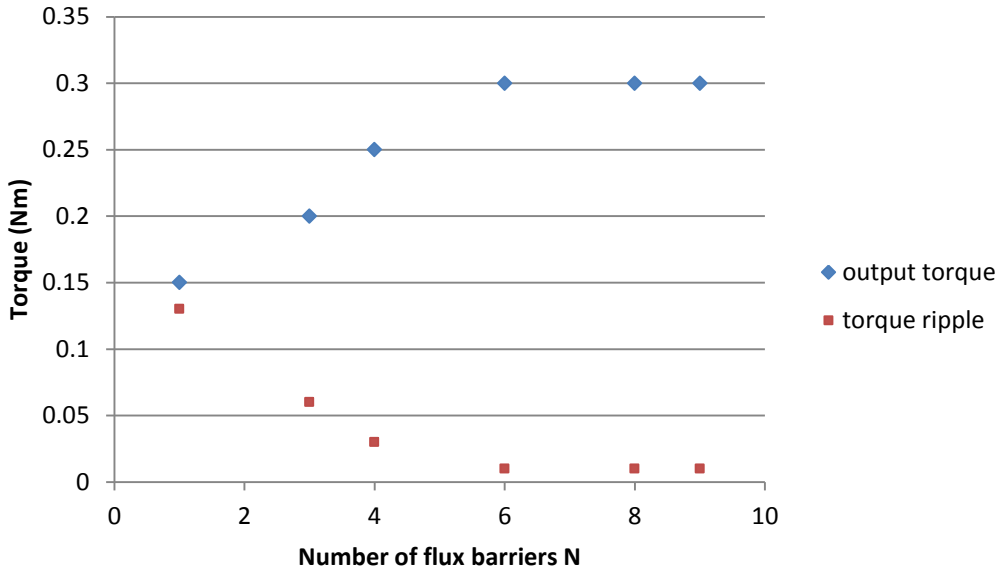

Figure 5.1 Relation between number of flux barriers and torque

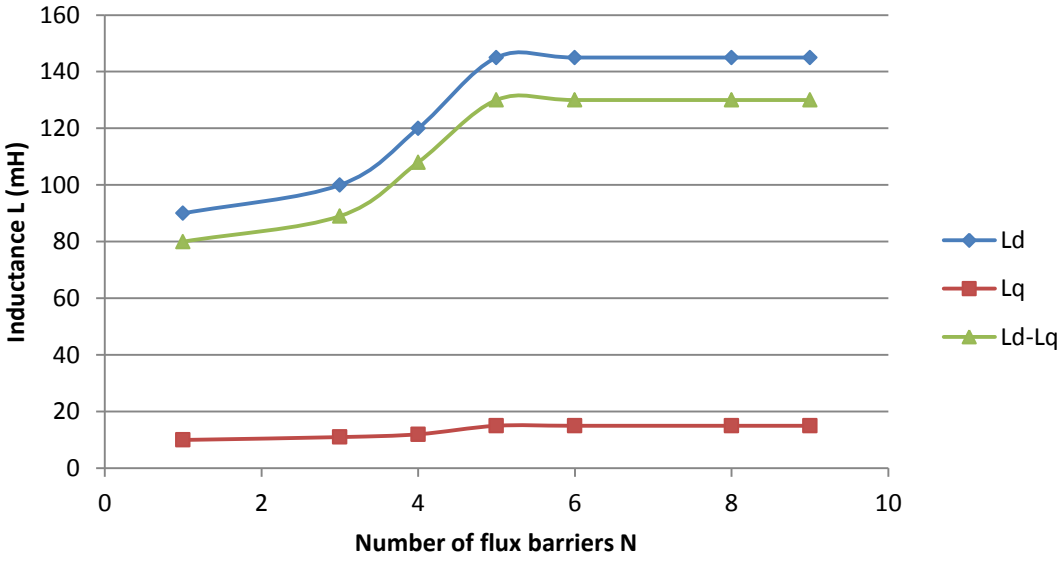

Figure 5.2 Relationship of Number of flux barriers and Inductance

5.2 b. Ratio of Insulation or flux barrier to iron rib width (K_w)

The studies regarding the rotor design optimization done by T.A. Lipo [5], two key variables in rotor construction are W_{iron} or the width of rotor segment or iron sheet and W_{ins} or the flux barrier or insulation width. The sum of $n(W_{iron}+W_{ins})$ is chosen as equal to the width of one stator tooth to limit the pulsating fluxes in stator teeth.

Simulations have been done for various values of K_w, and it has been realized that, if the value of K_w is 0.5, it is possible to obtain high motor torque index $L_d - L_q$ and Saliency Ratio. Thus 0.5 is chosen as an optimal value for K_w by considering the above results and constructional aspects. The figures 5.3 and 5.4 show the relation between K_w and motor torque index and with the saliency ratio.

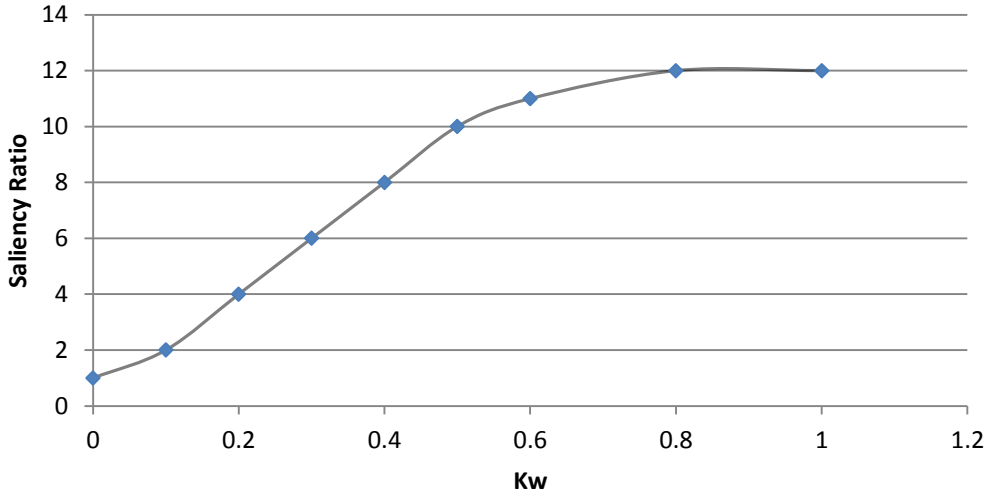

Figure 5.3 Relation between K_w and Saliency Ratio

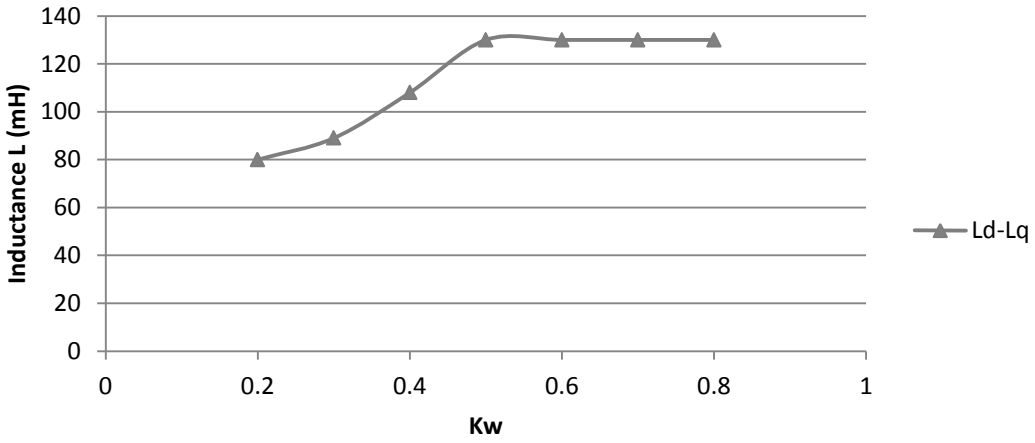

Figure 5.4 Simulated relationship between K_w and L_d - L_q

5.2 c. Stator configuration

In the design process, the d and q axis inductances and saliency ratio are independent of stator configuration. The figure 5.5 [5] pertaining to the effect of stator slot number shows that, the $L_d - L_q$ characteristics are independent of the stator configuration. The number of slots has very little effect on saliency ratio and motor torque index.

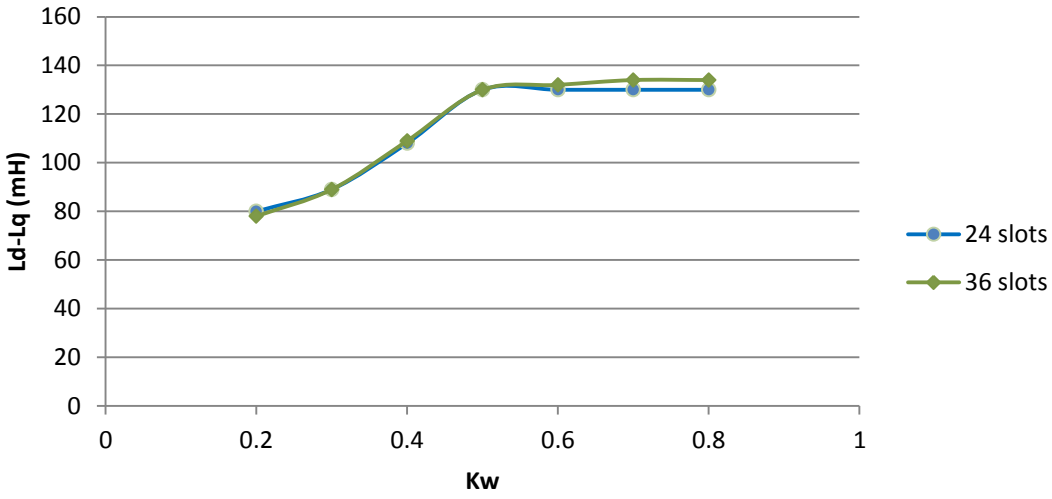

Figure 5.5 Relation between L_d-L_q and K_w

5.3 Final Design

From the results of the structural optimization techniques, a final design was done for a 300 W motor using FCSMEK. Some of the main parameters of the machine are given in table 5.1. The data file used in the FCSMEK program cim.data is given in Appendix A. The different dimensions of the rotor pole and stator slot are given in Appendix B. The finite element mesh is given in Appendix D.

Table 5.1 Motor Specifications

Outer Diameter of stator	50.5 mm	Stack Length	51 mm
Inner diameter of stator	30.8 mm	Number of poles	4
Outer diameter of rotor	30.5 mm	Rated Output	300 W
Shaft diameter	4.10 mm	Rated voltage	400 V
Number of stator slots	24	Rated torque	0.3 Nm
		Rated speed	10000 rpm

The time stepping analysis gives information about the losses of the motor. It has been shown that, the total electromagnetic loss is about 66 W. The losses data file is given in Appendix C. The motor has got an electrical efficiency of 83%.

5.4. Simulation Results

The flux density distribution of the motor is shown in figure 5.6. Figures 5.7, 5.8 and 5.9 shows the voltage, current and airgap torque plotting of the motor. The distribution of iron, resistive and total losses are shown in figures 5.10, 5.11 and 5.12.

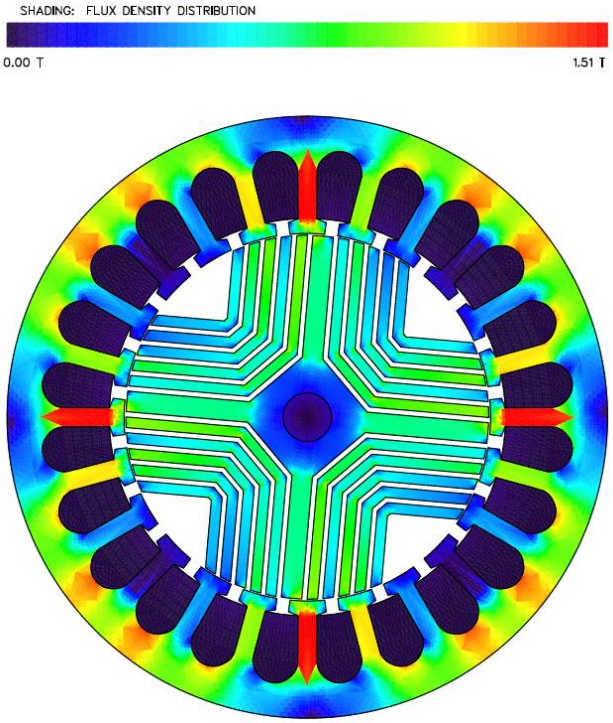

Figure 5.6 Flux density distribution in the rotor

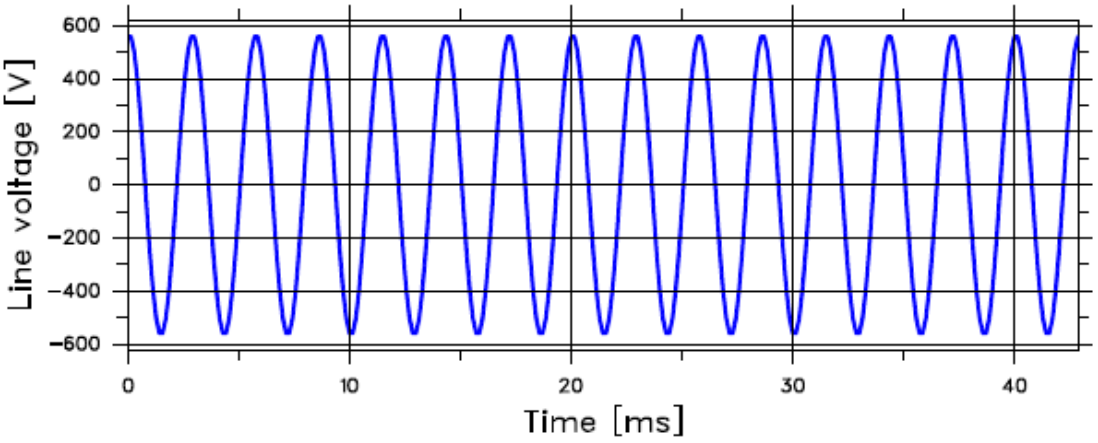

Figure5.7 Line Voltage

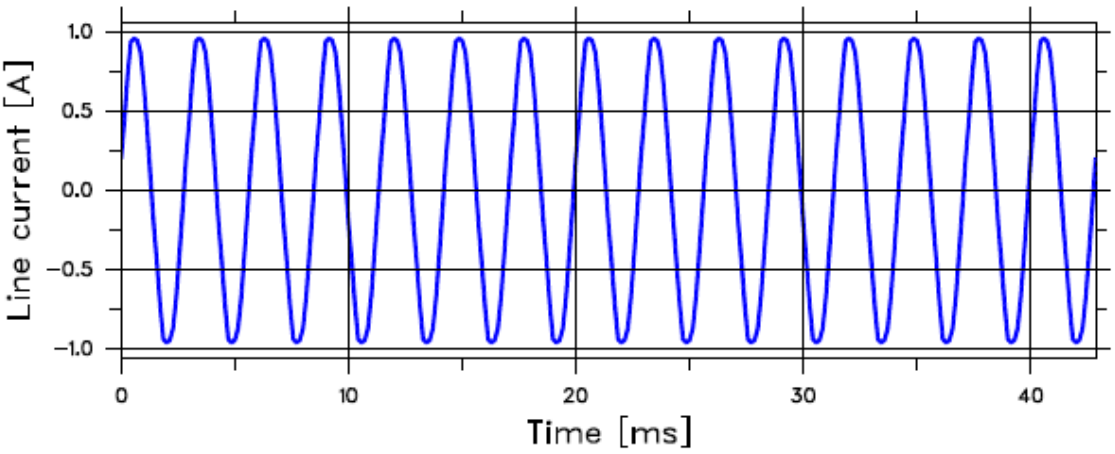

Figure 5.8 Line current

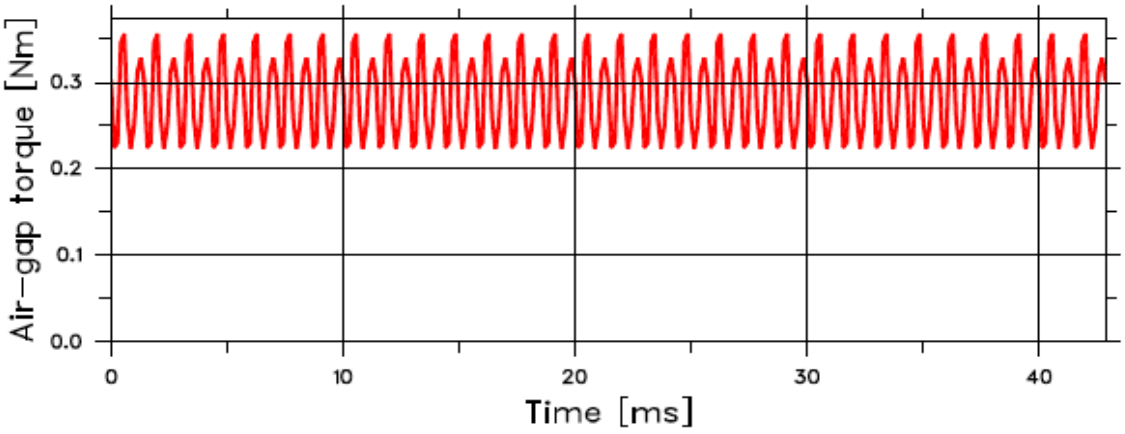

Figure 5.9 Air-gap torque

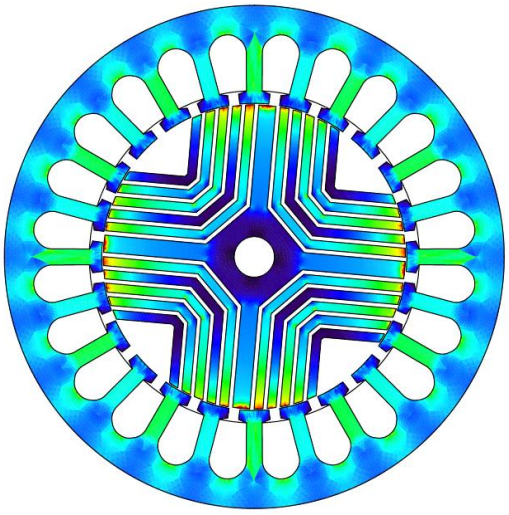

Figure 5.10 Iron loss distribution

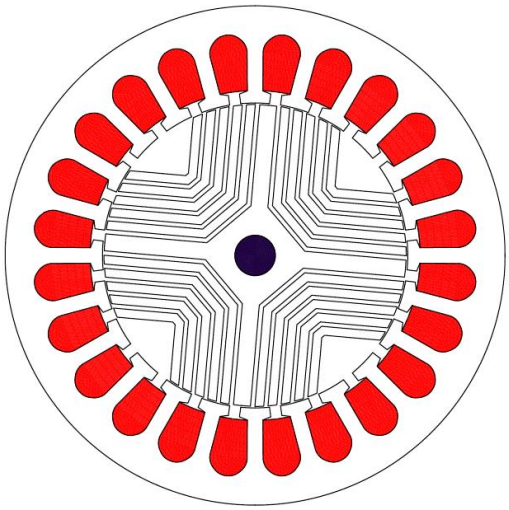

Figure 5.11 Distribution of resistive losses

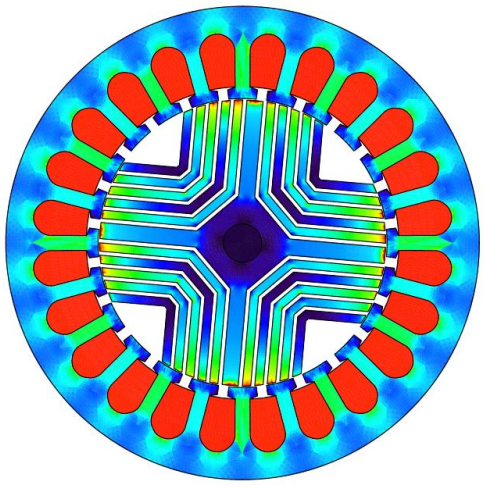

Figure 5.12 Total losses distribution

6. THERMAL MODELLING

In the process of design and optimization of electrical machines, thermal analysis is an integral part. In order to increase the energy efficiency and to reduce the cost and size of the machine, it is important to analyze the thermal behavior of the machine. Also, it facilitates the utilization of new materials and topologies in machine construction.

Here in this project, the thermal modeling was done using the references from works done by J. Saari, M. Kaltenbacher [10], Mohamad M. [11] and P.H Mellor [13].

In electrical motors, the electrical and mechanical losses cause the production of heat and in general, the heat flows from inner to the outer part of the machine. There are three modes by means of which heat can be transferred. Those are,

Heat Conduction

Heat Convection

Heat Radiation

6.1 Conduction

When there is a temperature gradient in a body, energy transfer occurs in it from high-temperature to low-temperature region. The heat transfer takes place by means of molecular collisions and vibrations. This mode of heat transfer is called conduction and which is the most considerable means of heat transfer within a solid or between solids. According to Fourier Law, the heat transfer is given by,

$$\frac{\Delta Q}{\Delta t} = -\lambda A \frac{dT}{dx} \tag{6.1}$$

where A(m^2) is the cross sectional area, λ(W/m.K) is the thermal conductivity of the material and dT/dx is the temperature gradient in the material.

The one dimensional thermal resistance between two points can be calculated by,

$$R_{\text{th}} = \frac{L}{\lambda A} \tag{6.2}$$

If the material is cylindrical in shape and it is assumed that there is only radial heat transfer.

Then,

$$R_{th} = \frac{\ln(r_0/r_i)}{\lambda L \varphi} \tag{6.3}$$

where φ is the angle of the sector and r_0 and r_i are the outer and inner radius of the cylinder in meters.

6.2 Convection

Thermal convection is the heat transfer from one place to another by movement of fluids or the the heat transfer between a surface and a fluid when there is a temperature gradient. Convection can be free or forced. When fluid motion is caused naturally by bouyancy forces and density variations in the fluid, it is callef free convection. When the fluid is forced to flow by means of external forces like a fan, it is then forces convection.

Heat exchange due to convection is given by,

$$q = hA(T_{env} - T) \tag{6.4}$$

where h (W/m^2 .K) is the heat transfer coeffiecient. It depends on the physical characterisitcs of the surface and the fluid.

T_{env} is the temperature of the environment.

T is the temperature of the solid.

The thermal resistance for convection is given by,

$$R_{\text{th}} = \frac{1}{hA} \tag{6.5}$$

6.3 Radiation

Thermal radiation is the heat dissipation to the environment by means of electromagnetic radiation. If the temperature is greater than absolute zero, all matters emits radiation.

The heat dissipation can be calculated by

$$q = A\varepsilon\sigma({T_s}^4 - {T_{amb}}^4) \tag{6.6}$$

where σ is Stefan-Boltzmann constant (σ = 5.67*10^{-8} W/m^2 . K^4) and ε is the surface emissivity ($0 < \varepsilon < 1$). T_s and T_{amb} are the surface and ambient temperature respectively.

Here, the thermal resistance to the suroundings is,

$$R_{th} = \frac{T_s - T_{amb}}{A\varepsilon\sigma({T_s}^4 - {T_{amb}}^4)} \tag{6.7}$$

6.4 Lumped Thermal Model

A lumped parameter thermal network for the synchronous reluctance motor under study is shown in figure 6.11. The methods behind the calculation of these thermal resistances are explained in the subsequent sections.

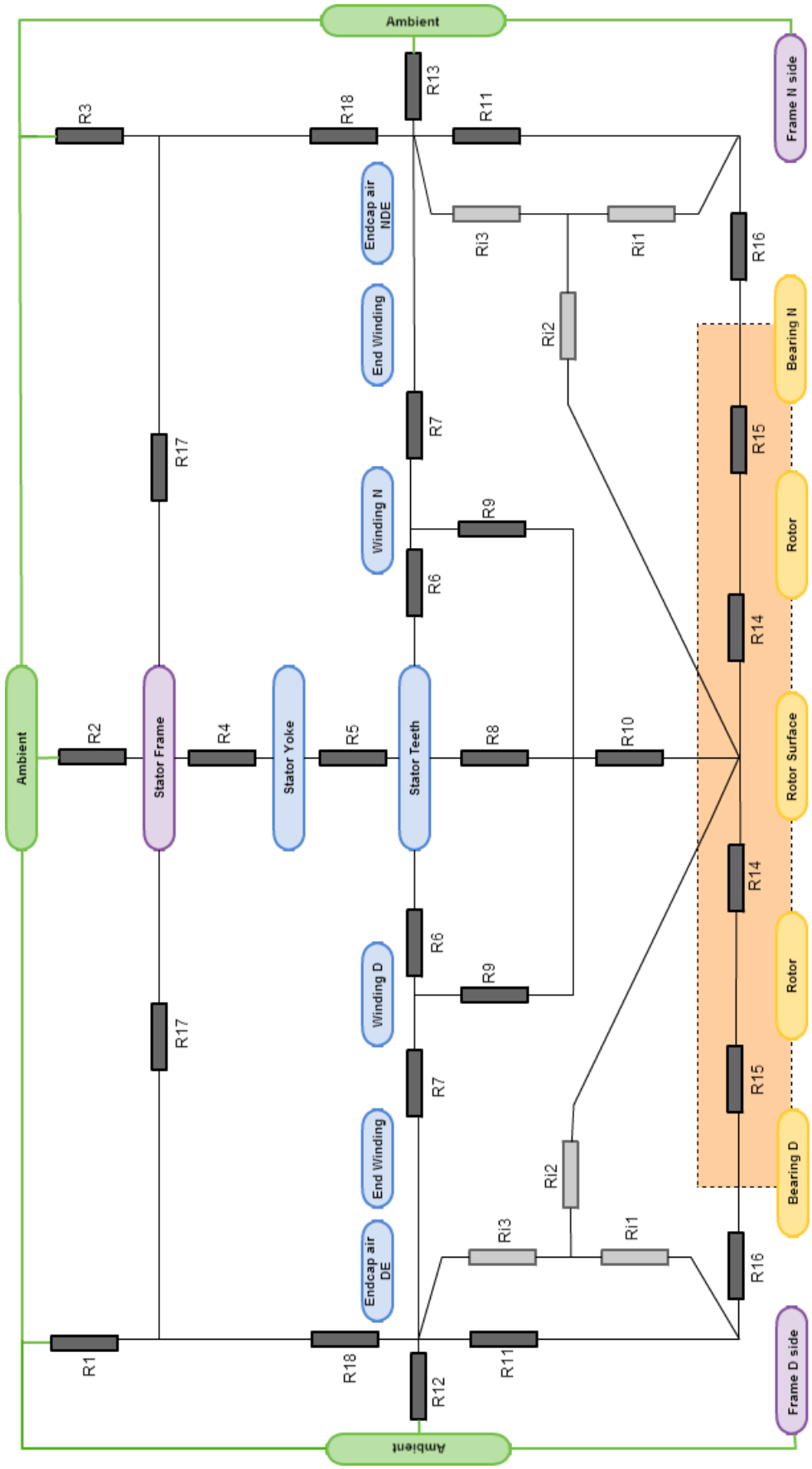

Figure 6.1 Lumped parameter Thermal Network of the Synchronous Reluctance Motor

6.5 Models of the Machine parts

6.5 a. Frame

The frame can be divided into five parts for thermal modeling. Those are endcap frame NDE (Non Drive End), ribbed frame over endcap air NDE, ribbed frame over stator yoke, ribbed frame over endcap air DE (Drive End) and endcap frame DE.

The thermal resistances and corresponding heat flows are given below

R_1 – Heat flow from the ribbed frame over endcap air to ambient at DE

R_3 - Heat flow from the ribbed frame over endcap air to ambient at NDE

R_2 – Heat flow from the ribbed stator surface frame to ambient

R_{11}, R_{18} – Axial heat flow between single parts

R_{12} – Heat flow from endcap frame DE to ambient

R_{13} - Heat flow from endcap frame NDE to ambient

R_4 – Thermal contact between stator yoke and frame

$$R_1 = \frac{1}{\frac{1}{R_{\text{fin}}(h_{\text{f4}}\, L_1\, b_{\text{r}}\, a_{\text{r}}\, \lambda_{\text{f}})} + h_{\text{f4}}\, S_{\text{f1}}} \tag{6.8}$$

$$R_3 = \frac{1}{\frac{1}{R_{\text{fin}}(h_{\text{f2}}\, L_1\, b_{\text{r}}\, a_{\text{r}}\, \lambda_{\text{f}})} + h_{\text{f2}}\, S_{\text{f1}}} \tag{6.9}$$

$$R_2 = \frac{1}{\frac{1}{R_{\text{fin}}(h_{\text{f3}}\, L_{\text{fe}}/k\, b_{\text{r}}\, a_{\text{r}}\, \lambda_{\text{f}})} + h_{\text{f3}}\, S_{\text{f2}}} \tag{6.10}$$

$$R_{17} = \frac{0.5 L_1}{\lambda_{\text{f}}\,(A_{\text{f}} + A_{\text{r}})} \tag{6.11}$$

$$R_{18} = R_{17} + \frac{1}{h_{\text{c2}}\, A_{\text{f}}} + \frac{0.25(D_{so} - D_{si})}{\lambda_{\text{f}}\, A_{\text{f}}} \tag{6.12}$$

$$R_{11} = \frac{0.25(D_{so} - D_s)}{\lambda_{\text{f}}\, A_{\text{f}}} \tag{6.13}$$

$$R_{12} = \frac{1}{h_{\text{f5}}\, S_{\text{fD}}} \tag{6.14}$$

$$R_{13} = \frac{1}{h_{\mathrm{f1}} S_{\mathrm{fN}}} \tag{6.15}$$

$$R_4 = \frac{1}{h_{\mathrm{c1}} S_{\mathrm{yo}}} \tag{6.16}$$

$$R_{16} = \frac{1}{4} R_{\mathrm{b}} \tag{6.17}$$

$$R_{15} = \frac{1}{4} R_{\mathrm{b}} + \frac{1}{2} R_{\mathrm{sh}} + \frac{1}{2} R_{\mathrm{r}} \tag{6.18}$$

$$R_{14} = \frac{1}{4} R_{\mathrm{r}} \tag{6.19}$$

$$R_{17} = \frac{0.5 L_1}{\lambda_{\mathrm{f}} \left(A_{\mathrm{f}} + A_{\mathrm{r}}\right)} \tag{6.20}$$

$$R_4 = \frac{1}{2} R_{\mathrm{fr2}} + \frac{1}{2} R_{\mathrm{y}} \text{ (Also, equation 6.16 can be used)} \tag{6.21}$$

$$R_5 = \frac{1}{2} R_{\mathrm{y}} + \frac{1}{2} R_{\mathrm{t}} \tag{6.22}$$

$$R_6 = \frac{1}{2} R_{\mathrm{w}} \tag{6.23}$$

$$R_7 = \frac{1}{2} R_{\mathrm{ew}} \tag{6.24}$$

λ_{f} - Specific thermal conductivity of frame

h_{c1}- Heat contact coefficient between stator yoke and frame

h_{c2}- Heat contact coefficient between frame middle and endcap frame

h_{f1}- Heat contact coefficient from endcap frame NDE to ambient

h_{f2}- Heat contact coefficient from ribbed frame over endcap air NDE to ambient

h_{f3}- Heat contact coefficient from ribbed frame over stator core to ambient

h_{f4}- Heat contact coefficient from ribbed frame over endcap air DE to ambient

h_{f5}- Heat contact coefficient from endcap air DE to ambient

k – Stacking factor

L_{fe} – Effective length of stator core

L_1 - Length of rib over endcap air

a_{r} – Thickness of frame rib

b_{r} – Height of frame rib

D_{so} – Outer diameter of stator yoke

D_s – Diameter of shaft

S_{f1} – surface of frame between the ribs over endcap air

S_{f2} – surface area of frame between the ribs over stator core

S_{yo} – outer surface area of stator yoke S_{fN} - frame surface area of endcap frame NDE

S_{fD} - frame surface area of endcap frame DE

A_f - cross sectional area of frame A_r – cross sectional area of ribs

6.5 b. Stator Yoke

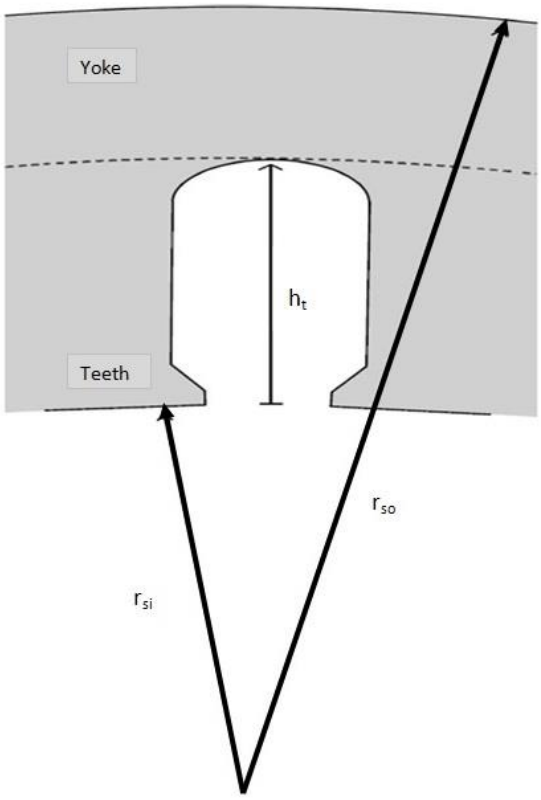

Figure 6.2 Stator Yoke shape

The equivalent thermal resistance of the stator yoke can be calculated using the formula, but considering the geometry given in figure 6.2, the resistance can be determined by,

$$R_{\text{yoke}} = \frac{\ln(r_{\text{so}}) - \ln(r_{\text{si}} + h_t)}{2\pi\lambda L_{act}} \tag{6.25}$$

where, r_{so} and r_{si} are the outer and inner diameter of the stator.

6.5 c. Stator Teeth

The geometry of the tooth is such that the area of the tooth varies with height. Hence, the corresponding thermal resistance needs to be integrated.

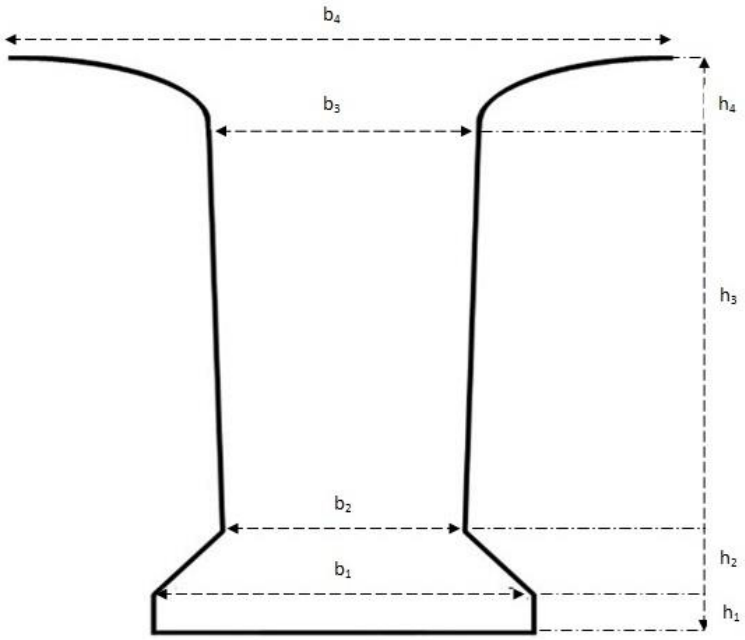

Figure 6.3 Shape of stator teeth

$$R_t = \int_0^h \frac{1}{Q_s \, \lambda \, L_{\text{act}} \, b(h)} \, dh \tag{6.26}$$

Q_s -Number of stator slots

The integration can be made over half the tooth and divide the final result by two.

$$R_{\text{t}} = \frac{1}{2Q_{\text{s}} \, \lambda \, L_{\text{act}}} \left[\frac{2h_1}{b_1} + \frac{2h_2}{b_2 - b_1} \ln \frac{b_2}{b_1} + \frac{2h_3}{b_3 - b_2} \ln \frac{b_3}{b_2} + \text{Arc} \right] \tag{6.27}$$

where,

$$\text{Arc} = \frac{2h_4}{b_4 - b_3} \left[-\frac{\pi}{2} + \frac{k}{\sqrt{k^2 - 1}} \tan^{-1} \left(\frac{1}{\sqrt{k^2 - 1}} \right) \right] \tag{6.28}$$

The derivation for equation is given in Appendix E.

6.5 d. Stator Winding

The stator slot shape can be transformed into a rectangle in order to calculate the thermal resistance.

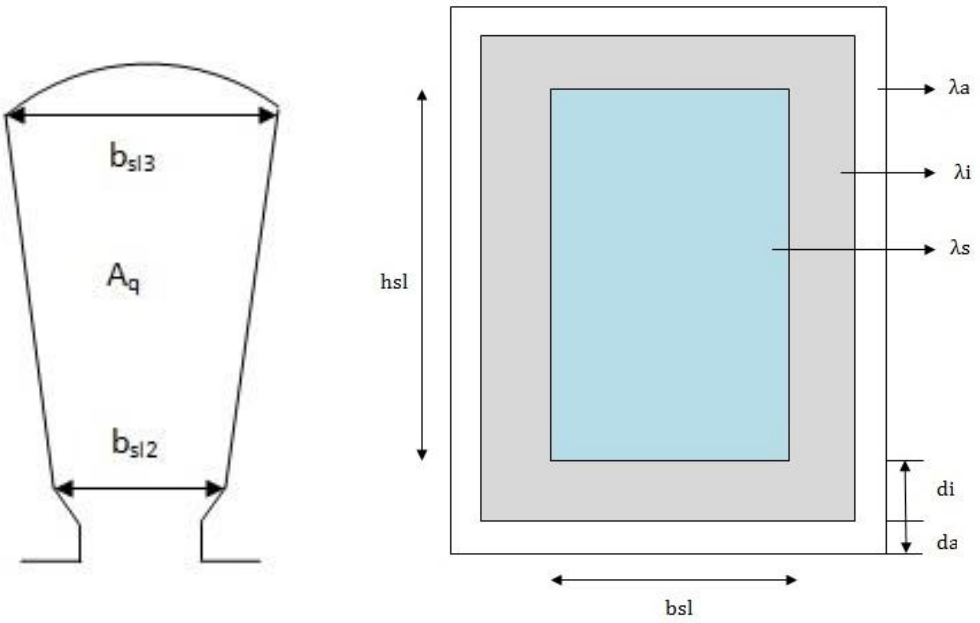

a. Real slot area b. Equivalent slot area

Figure 6.4 Stator winding dimensions

d_A – equivalent height of the air between the insulation and teeth and given to be around 0.3 mm [12]

d_I – length of the insulation

$$d = dI + dA \tag{6.29}$$

$$b = \frac{b_{sl3} + b_{sl2}}{2} - 2d \tag{6.30}$$

$$h = \frac{2A_Q}{b_{sl3} + b_{sl2}} - 2d \tag{6.31}$$

Inside the winding area, the heat dissipation can be calculated by,

$$R_{x0} = \frac{b}{h\lambda_s} \tag{6.32}$$

$$R_{y0} = \frac{h}{b\lambda_s} \tag{6.33}$$

where, λ_s – equivalent slot thermal conductivity, and which is dependent on the fill factor of the machine as per the figure 6.5 [12]

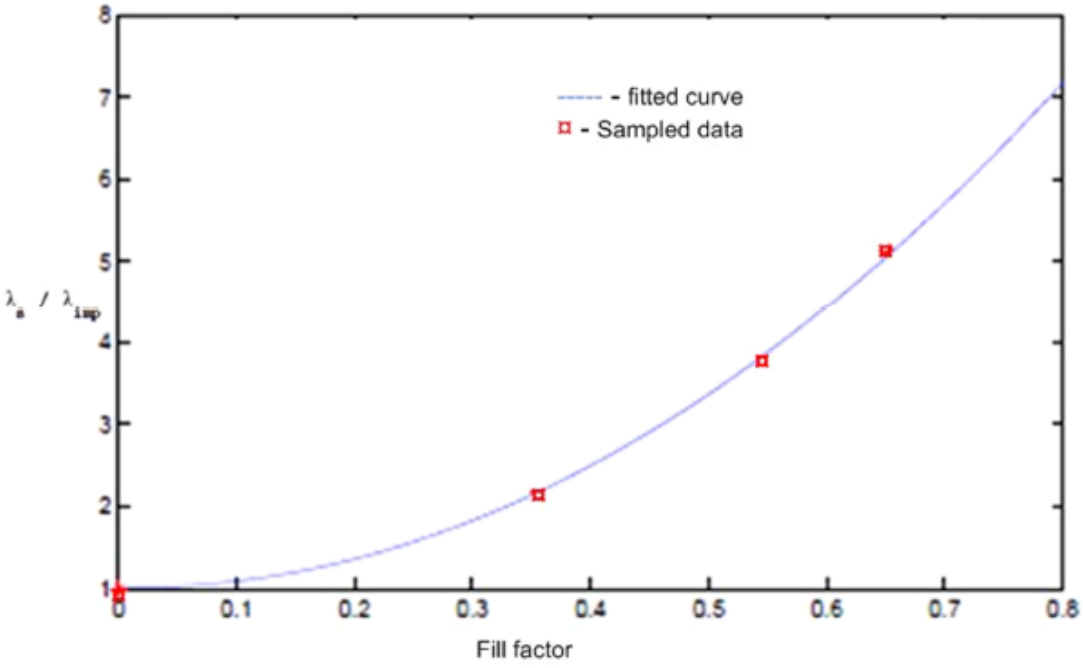

Figure 6.5 Relation between fill factor and thermal conductivity

When the insulation material and air film are taken into consideration, the heat dissipation is given by,

$$R_{ix} = \frac{d_I}{h\lambda_1} + \frac{d_A}{h\lambda_A} \tag{6.34}$$

$$R_{iy} = \frac{d_I}{b\lambda_1} + \frac{d_A}{b\lambda_A} \tag{6.35}$$

The above for equations are arranged together, then,

$$R_{\mathrm{y}} = \frac{1}{2}\left(R_{\mathrm{iy}} + \frac{R_{\mathrm{y0}}}{6}\right) \tag{6.36}$$

$$R_x = \frac{1}{2}\left(R_{\mathrm{ix}} + \frac{R_{\mathrm{x0}}}{6}\right) \tag{6.37}$$

Then finally, the thermal resistance of the winding can be calculated by,

$$R_w = \frac{R_{\mathrm{x}}R_{\mathrm{y}}}{Q_s L\left(R_{\mathrm{x}} + R_{\mathrm{y}}\right)}\left(1 - \frac{R_{\mathrm{x0}}R_{\mathrm{y0}}}{720R_{\mathrm{x}}R_{\mathrm{y}}}\right) \tag{6.38}$$

6.5 e. End Winding

The thermal resistance of the end winding can be calculated using the formula [12],

$$R_{\mathrm{ew}} = \frac{l_{\mathrm{av}}}{\lambda_{cu}\, A_{cu}\, Q_s\, 6} \tag{6.39}$$

l_{av} – Half of the average length of the coil

This length can be approximately calculated as,

$$l_{\mathrm{av}} = L_{act} + 1.2\,\tau_{\mathrm{p}} + l' \tag{6.40}$$

where, τ_{p} – pole pitch and l' is empirically 0.05m for small machines

6.5 f. Air Gap

The thermal resistance in the air gap can be divided into three resistances, which are the resistances from the rotor surface to the air gap, from the air gap to the stator teeth and from the air gap to the stator winding.

Resistance from air gap to stator teeth is,

$$R_8 = \frac{1}{2h_{\mathrm{ag}}a_{\mathrm{st}}L_{\mathrm{fe}}Q_{\mathrm{s}}} \tag{6.41}$$

Resistance from air gap to the stator winding is,

$$R_9 = \frac{1}{2h_{\mathrm{ag}}a_{\mathrm{so}}\frac{L_{\mathrm{fe}}}{k}Q_{\mathrm{s}}} \tag{6.42}$$

Resistance from rotor surface to the air gap is,

$$R_{10} = \frac{1}{2h_{\mathrm{ag}}r_{\mathrm{ro}}\pi L_{\mathrm{fe}}} \tag{6.43}$$

Where, h_{ag} is the heat transfer coefficient between stator and rotor and a_{st} is the width of stator tooth. a_{so} – slot opening width, r_{ro} - outer radius of rotor

6.5 g. Rotor

The thermal resistance of the rotor R_r is calculated according to the theory and principles by [14]. In SRM, there are flux barriers of air in the rotor. As per the Computational Fluid Dynamics (CFD) studies done by [15], there is no air flow from one side to the other side of the rotor. Hence, there is heat transfer through natural conduction only. Compared to the air in the flux barriers, the thermal conductivity of rotor iron is much higher, and hence the convectional heat transfer can be neglected.

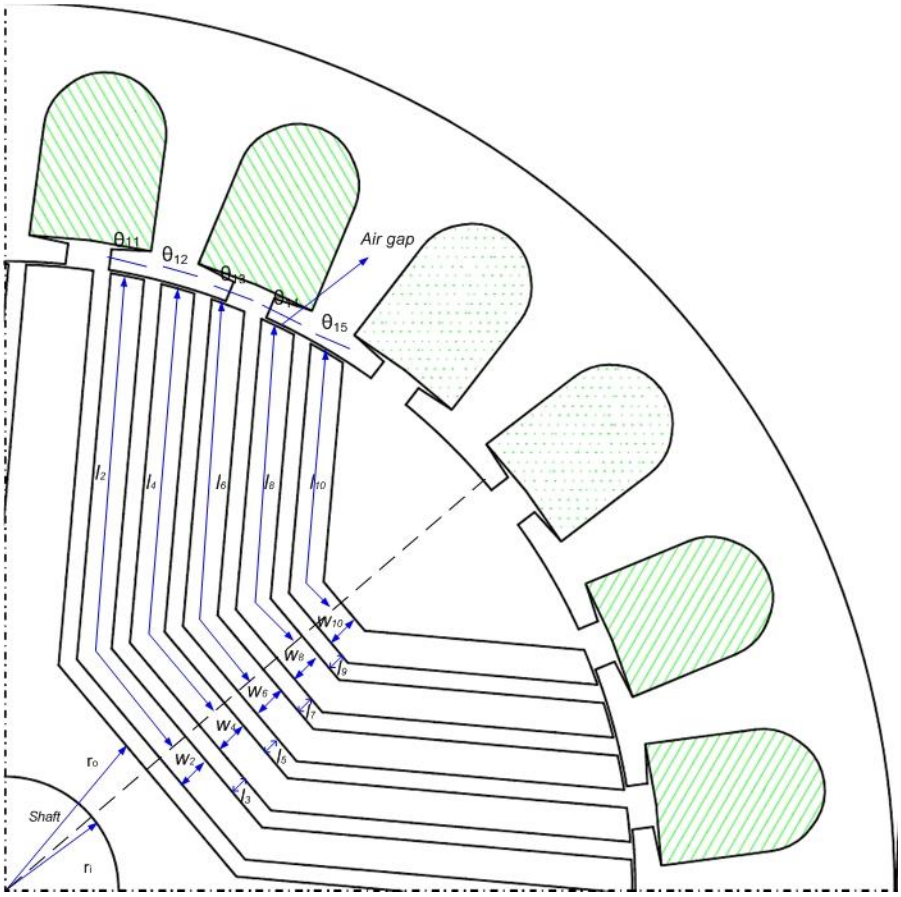

Figure 6.6 Rotor parameters dimensioning

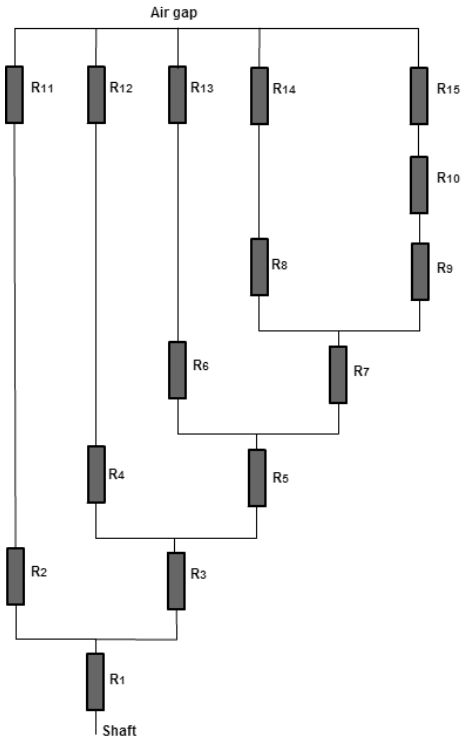

Figure 6.7 Thermal resistances of rotor portions

The figure 6.6 depicts the principle behind the calculation of rotor thermal resistance.

For resistances from R_2 to R_9, the thermal resistance can be calculated using the equation 6.2 for one dimensional resistance between two points,

$$R_{\text{th}} = \frac{L}{\lambda A} \tag{6.44}$$

While the resistances R_1 and R_{10} to R_{14} are calculated by equation 6.3,

$$R_{\text{th}} = \frac{\ln(r_0/r_i)}{\lambda L \varphi} \tag{6.45}$$

6.5 h. Shaft

The thermal resistance of the shaft can be calculated using the equation

$$R_{sh} = \frac{l_{\text{sh}}}{\pi {r_{\text{sh}}}^2 \lambda_{\text{sh}}} \tag{6.46}$$

l_{sh} – Length of the shaft from one bearing to the other

r_{sh} – Outer radius of the shaft

λ_{sh} – Thermal conductivity of the shaft

6.6 Convection Heat Transfer

6.6 a. Internal Air to Frame

According to [11] and [12], the heater transfer from the air inside the motor to the inside frame area can be calculated using the formula,

$$R_{i1} = \frac{1}{\alpha_1 A_1} \tag{6.47}$$

A_1- Area exposed to the internal air

$$A_1 = \pi \left[r_s^{\,2} + r_s \left(l_{\text{sh}} - l_{\text{fe}} \right) \right] \tag{6.48}$$

where the heat transfer coefficient α_1 is given by,

$$\alpha_1 = k_1 + k_2 \left(\frac{\omega}{v_0} r_r \right)^{0.65} \tag{6.49}$$

α represents both conduction and convection.

where,
ω is the angular velocity and $v_0$is the velocity in meter per second.

$k_1 = 15\ \text{W/m}^2\text{K}$

$k_2 = 3.45\ \text{W/m}^2\text{K}$

$$ie: \quad \alpha_1 = 15 + 3.45 \left(\frac{\omega}{v_0} r_r \right)^{0.65} \tag{6.50}$$

$r_s -$ Stator outer radius

r_r - Rotor outer radius

l_{sh} - Shaft length

l_{fe} - Stack length

6.6 b. Internal Air to Rotor

As per [12], the heat transfer due to convection between internal air and rotor wings can be calculated using the empirical relation,

$$R_{i2} = \frac{1}{\propto_2 A_2} \tag{6.51}$$

Where,

$\propto_2 = 6.16 \left(\frac{\omega}{v_0} r_r \right)^{0.65}$

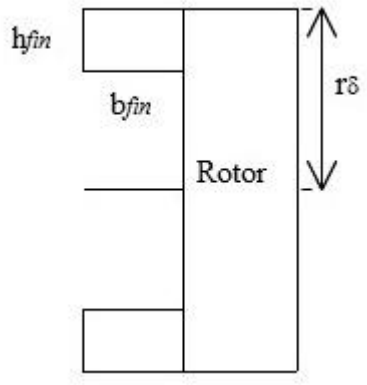

Figure 6.8 Area of the Rotor wings

$r_i -$ Inner radius of rotor

The area $A_2 = 2\, b_{fin}\, h_{fin}\, \eta_{fin} + \pi {r_\delta}^2$

$$r_\delta = \frac{r_i + r_r}{2} \tag{6.52}$$

where, h_{fin} (m) and b_{fin} (m) are the height and width of the rotor fins

η_{fin}-Number of fins r_δ(m) – Average airgap length

6.6 c. End winding to internal air

The space between the end windings and the internal air has got a thermal resistance which can be calculated by,

$$R_{i3} = \frac{1}{\propto_3 A_3} \tag{6.53}$$

$$\propto_3 = 6.5 + 2.70 \left(\frac{\omega}{v_0}\, r_r \right)^{0.6} \tag{6.54}$$

$$A_3 = A_\propto + A_\beta + A_\gamma + A_\delta + A_\epsilon \tag{6.55}$$

Different areas are portrayed in Figure 6.9

$$A_\propto = \pi\, ({r^2}_{ho} - {r^2}_{hi}) \tag{6.56}$$

$$A_\beta = 2\pi\, r_{ho}\, l_h \tag{6.57}$$

$$A_\gamma = 2\pi\, r_{hi}\, l_h \tag{6.58}$$

$$A_\delta = Q_s\, 2\pi\, r_{lk}\, l_{hs} \tag{6.59}$$

$$A_\varepsilon = A_\alpha - Q_s\, \pi\, {r^2}_{lk} \tag{6.60}$$

r_{lk} is calculated from the average copper area

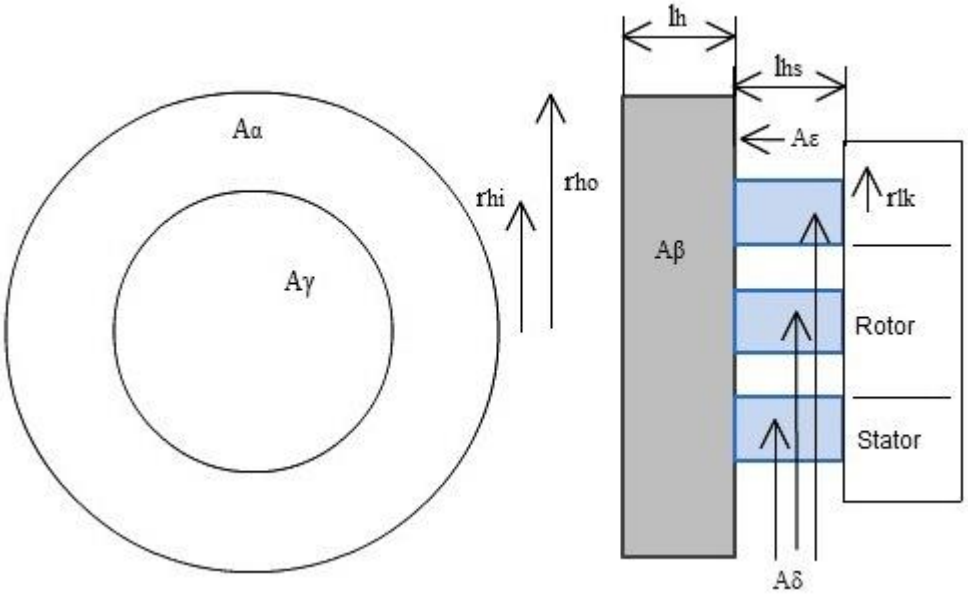

Figure 6.9 Calculation of end winding surface area

6.7 Thermal Analysis Results

6.7 a. Losses and Thermal Resistances in major parts of the motor

Stator Losses

P_{yoke} = 10.18 W

P_{teeth} = 9.93 W

$P_{winding}$ =33.2 W

Rotor Loss

P_{yoke} = 11.46 W

6.7 b. Thermal resistances (K/W) from the lumped parameter thermal modeling

Stator Yoke R_{yoke} = 0.017

Stator teeth R_{teeth} = 0.018

Stator winding R_w = 0.155

Enwinding R_{ew} = 0.062

Rotor R_r = 0.492

Shaft R_{sh} = 0.232

Frame R_{fr} = 0.126

6.7 c. The resistances inside the stator and rotor body

Table 6.1 Thermal Resistances

R_1	=0.044	R_{10}	=0.712
R_2	=0.251	R_{11}	=0.031
R_3	=0.034	R_{12}	=0.512
R_4	=0.072	R_{13}	=0.532
R_5	=0.080	R_{14}	=0.125
R_6	=0.061	R_{15}	=0.362
R_7	=0.027	R_{16}	=0.004
R_8	=0.650	R_{17}	=0.041
R_9	=0.700	R_{18}	=0.082

The thermal conductivities and heat transfer coefficients used in the calculations are given below:

Steel λ=52 W/mK

Stator Slot λ=4.5 W/mK

Copper λ=370 W/mK

Air λ=0.028 W/mK

Aluminium λ=240 W/mK

Heat transfer coefficient between stator and rotor h_{ag}= 100 W/m^{2}K

Heat transfer coefficient from stator yoke to frame h_{c1} = 30 W/m^{2}K

Heat transfer coefficient from end cap air to ambient h_{f5}=200 W/m^{2}K

The thermal network can be solved by setting up equation in accordance with Kirchhoff Current Law (KCL).

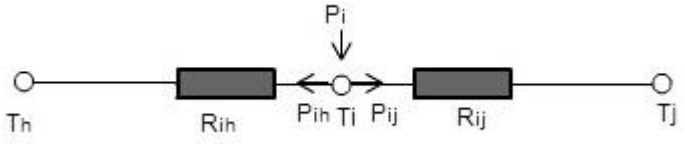

Figure 6.10 Heat flow

Now,

$$P_{\mathrm{i}} = \frac{T_{\mathrm{i}} - T_{\mathrm{j}}}{R_{\mathrm{ij}}} + \frac{T_{\mathrm{i}} - T_{\mathrm{h}}}{R_{\mathrm{ih}}}$$

The values of temperature rise in some of the parts are given below:

Rotor	= 35.5°C
Stator teeth	= 48.5°C
Stator yoke	=41.6°C
Stator winding	=64.1°C

7. Project Outcome

7. 1. Results and Conclusion

The major aim of the project has been met by conducting a detailed study on the features and performance of high speed low power synchronous reluctance motor and analyzed how it suits the needs of household applications. Besides, some of the design parameters and their effect on motor performance have been identified by doing finite element analysis and simulation experiments.

From the project work, it has been found out that, Synchronous reluctance motors are feasible alternative for induction motors while performance is considered and also, SRMs can be put in place of permanent magnet motors where cost effectiveness is a matter of concern. One of the main features of the SRM is the reduced losses when compared to induction motors and also, low temperature rise while operation.

7.2. Future Work

The project has been done in simulation level experiments and analytical calculations. There has been no practical manufacturing or testing of the machine under study. For accurate analysis of machine operational parameters, performance and thermal behavior, practical testing has to be carried out. Some of the subsequent works in this project are,

- Constructing prototypes of the motor in order to compare the performance with Induction and Permanent magnet motors and to estimate the temperature rise, by doing laboratory testing.
- Modification of stator design according to the rotor structure to get the optimum torque by considering the aspects of frequency converter also comes under the research.
- To develop energy efficiency design and optimization algorithms for Synchronous Reluctance Motor and to build Finite Element Models for different rotor designs.
- To find out possible ways to reduce the torque ripple and fault effect analysis of the motor under various operation conditions are other areas.

8. REFERENCES

[1] D.A. Staton, T.J.E. Miller, S.E. Wood, "Maximizing the saliency ratio of the synchronous reluctance motor", IEEE proceedings-B, Vol. 140, No.4, July 1993

[2] I.Boldea, Reluctance Synchronous Machines and Drives, Published: Oxford : Clarendon Press, 1996.

[3] J. K. KOSTKO: "Polyphase reaction synchronous motors", Journal Amer. Inst. Elect. Engrs, 1923, Vol 42, pp. 1162-1168.

[4] Hiroyulu Kinyama, Shinichiro Kawano, Yukio Hond, Toshiro Higaki, Shigeo Morimoto, Yoji Takeda, "High Performance Synchronous Reluctance Motor with Multi-flux Barrier for the Appliance Industry", in proc. Industry Applications Conference, 1998. Thirty-Third IAS Annual Meeting. The 1998 IEEE Volume: 1, Page(s): 111 - 117 vol.1

[5] Takayoshi Matsuo, Thomas A. Lipo, "Rotor Design Optimization of Synchronous Reluctance Machine", IEEE Transactions on Energy Conversion, Vol. 9. No. 2, June 1994

[6] Melissa Mila Naghibian, "A Maximum Torque per Ampere Vector Control for Synchronous Reluctance Machine Considering Saturation and Cross-Coupling Effects", Master of Science Thesis, KTH, Stockholm, Sweden May 2007

[7] J.J. Germishuizen, F.S. Van der Merwe, K. Van der Wetshuizen, M.J. Kamper, Performance Comparison of Reluctance Synchronous and induction traction drives for multiple units, in proc. Industry Applications Conference, 2000. Conference Record of the 2000 IEEE, Page(s): 316 - 323 vol.1

[8] T.A. Lipo, Synchronous Reluctance Machines – A viable alternative for AC Drives? Electric Machines and Power Systems, 19:659-671, 1991

[9] Aldo Boglietti, Michele Pastorelli, Induction and Sychronous Reluctance motor Comparison, in proc. Industrial Electronics, 2008. IECON 2008. 34th Annual Conference of IEEE, 10-13 Nov. 2008, Page(s) 2041 - 2044

[10] Kaltenbacher M., Saari J., An Asymmetric thermal model for totally enclosed fan-cooled induction motors, Report 38, Helsinki University of Technology, Laboratory of Electromechanics, Espoo, Finland

[11] Mohamad Mahmodui , Thermal Modelling of the Synchronous Reluctance Machine, Master Thesis, Electrical Machines and Power Electronics, School of Electrical Engineering, Royal Institute of Technology (KTH), Stockholm, Sweden 2012

[12] Gunnar Kylander. Thermal modelling of small cage induction motors. Doctoral thesis, Department of Electrical Machines and Power Electronics, CTH, Goteborg, Sweden, February 1996.

[13] P.H. Mellor, D. Roberts, D.R. Turner. Lumped parameter Thermal Model for Electrical Machines of TEFC Design. IEEE proceedings-B, Vol. 138, No.5, September 1991

[14] David A. Staton and Andrea Cavagnino, Convection Heat Transfer and Flow Calculations Suitable for Electric Machines Thermal Models, IEEE transactions on industrial electronics, vol. 55, no. 10, October 2008

[15] ABB CRC internal Reports

[16] A. Arkkio. Seminar on Electromechanics (Reluctance Machines) S-17. 3040, Lecture Notes, Aalto University.

Appendix A

```
Napa 51                                                    Version 2.0

       1              Machine type
       4              Number of poles
      350.            Frequency of the supply voltage

       0.051          Effective (airgap) length of the machine
       0.050          Length of the stator core
       0.050          Length of the rotor core
       0.             Length of the permanent magnets

     50.50E-03        Outer diameter of the stator core
     30.80E-03        Inner diameter of the stator core
       0              Index for the frame
       4              Index for the shape of stator slots
      24              Number of stator slots

       7.07E-03       H1   (Dimensions of the stator slots;
       1.00E-03       H11   see the maps of the slots)
       0.0            H12
       3.90E-03       H13
       0.0            H14
       0.0            H15
       1.10E-03       B11
       2.80E-03       B12
       3.80E-03       B13
       0.0            B14
       0.0            B15

      30.50E-03       Outer diameter of the rotor core
       4.10E-03       Inner diameter of the rotor core
       0.50           Moment of inertia of the rotor
      51              Index for the shape of rotor poles
       0              Index for the shape of damping bars
       6              Number of damping bars per pole
       0              Number of slots for the field winding
       0              Every second pole-shoe is a mirror image?
(0=No, 1=Yes)

       2.08E-03       H0   (Dimensions of the rotor pole;
       0.0            H01   see the maps of the poles)
       0.0            H02
       0.0            H03
       0.0            H04
       0.0            H05
       0.87E-03       B01
       0.45E-03       B02
       0.86E-03       B03
       0.0            B04
       0.0            B05

       0.0            H2   (Dimensions of the damping bars;
       0.0            H21   see the maps of the bars)
       0.0            H22
       0.0            H23
       0.0            H24
       0.0            H25
```

```
        0.0             B21
        0.0             B22
        0.0             B23
        0.0             B24
        0.0             B25

        3               Material index for the stator core
        0               Material index for the stator slot wedges
        3               Material index for the rotor pole shoes
        0               Material index for the opening of the damping
bars
        3               Material index for the rotor ring
        1               Material index for the centre of the rotor
       11               Material index for the stator coils
        0               Material index for the damping bars

        3               Number of phases
        1               Number of parallel paths in stator winding
       90               Number of conductors in a stator slot
        1               Number of layers of the stator winding
       12               Coil pitch in slot pitches
       18.626           Resistance of a stator phase
        1.662           End-winding reactance of a stator phase at 50
Hz
       22.              Temperature associated with the resistance
(C)

        0.320           Half of the average length of a coil
        0.6             Filling factor of a stator slot
        0.        H40   (Parameters of stator end winding)
        0.        H41
        0.              H42
        0.              H43

        0               Number of parallel paths in field winding
        0.              Turns per pole in the field winding
        0.              Resistance of the field winding
        0.              End-winding reactance of the field winding at
50 Hz
        0.              Temperature associated with the resistance
(C)

        0.              Average length of a turn in the field winding
        0.              Wide of a conductor in the field winding
        0.              Height of a conductor in the field winding
        0.              H50 (Parameters of the field winding)
        0.              H51
        0.              H52
        0.              Cross-sectional area of the end-ring
        0.              Radial height of the end-ring
        0.              Average diameter of the end-ring
        0.              Length of the rotor bars outside the core
(one end
        0.              Skew of rotor slots in stator slot pitches

        0               Additional parameters (Integers)

        0.              Additional parameters (Real numbers)
```

Appendix B

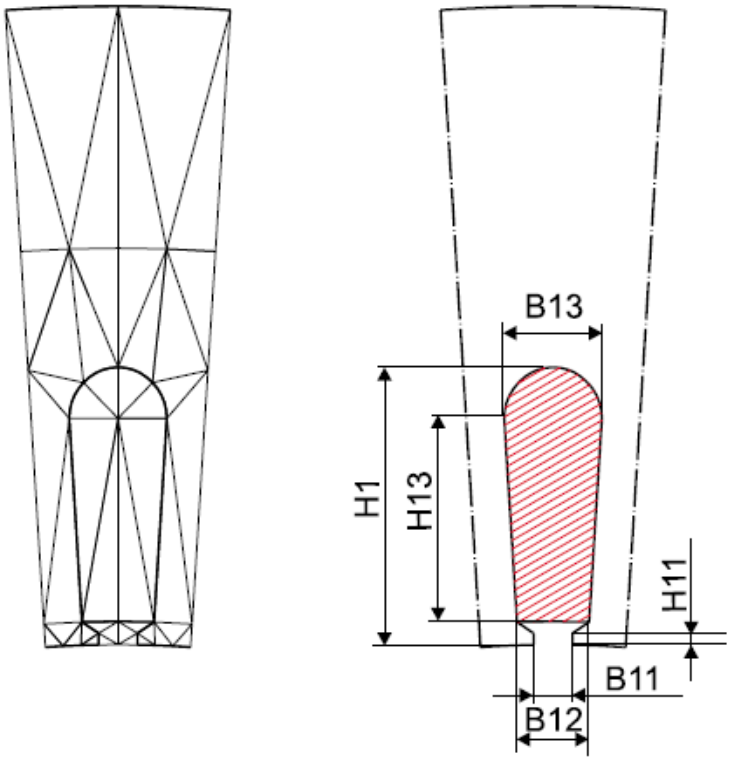

Figure B.1 Stator slot parameters

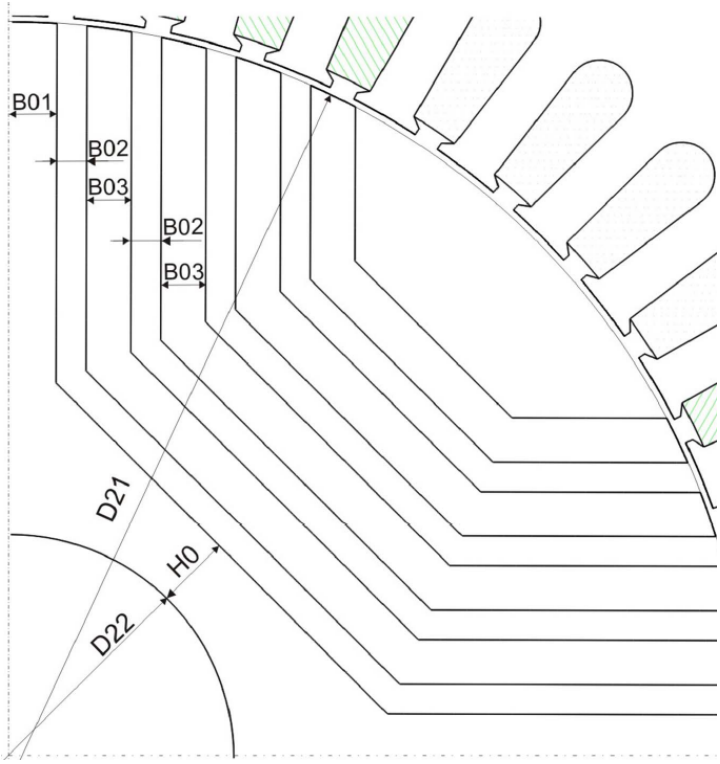

Figure B.2 Rotor Pole

Appendix C

Napa 51

```
*********   Effective and average values   *********
**************************************************

Integration period from     51.43 ms  to    57.14  ms


E.M.F. of the line                          400.00  V
Supply frequency                            350.00  Hz

Connection                                    STAR
Terminal voltage                            400.00  V
 - fundamental harmonic                     400.00  V
 - peak  value                              564.91  V
Terminal current                              0.70  A
 - fundamental harmonic                       0.69  A
 - peak value                                 0.97  A
Power factor                                0.6490
 - displacement factor                      0.6624  Ind.

Slip                                          0.000 %
Rotational speed                          10500.00  rpm
Air-gap torque                             283.183  Nmm
Shaft power                                 311.38  W
Air-gap flux density                          0.484 T

Stator temperature                           80.0   C
Current density in a stator slot              3.36  A/mm**2
Resistive losses in the st. winding          33.20  W
 - core region (d.c. resistance)              5.29  W
 - core region (skin-effect)                  0.03  W
 - end windings                              27.88  W
Core losses in the stator                    20.97  W
 - yoke                                      10.18  W
 - teeth                                      9.93  W
 - tooth tips                                 0.86  W

Rotor temperature                            80.0   C
Total resistive loss of the rotor             0.00  W
Resistive losses in other rotor parts         0.00  W
Core losses in the rotor                     11.46  W
 - yoke                                      11.46  W
 - teeth                                      0.00  W
 - tooth tips                                 0.00  W


Stator losses                                54.16  W
Rotor losses                                 11.46  W
Total electromagnetic loss                   65.62  W
```

Appendix D

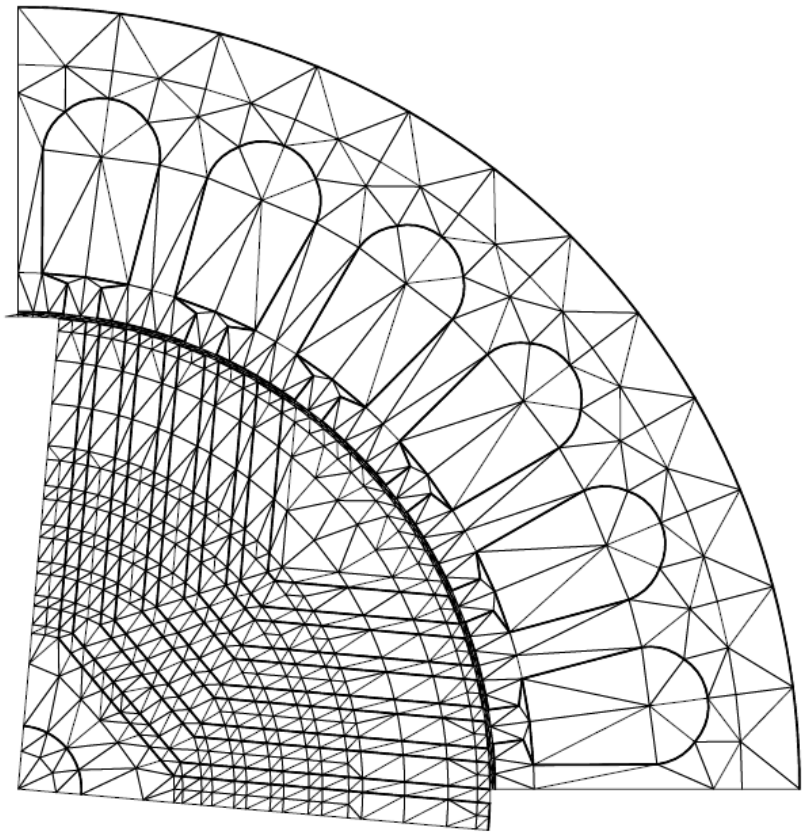

MACHINE TYPE: Napa 51
2943 NODES, 1342 ELEMENTS.

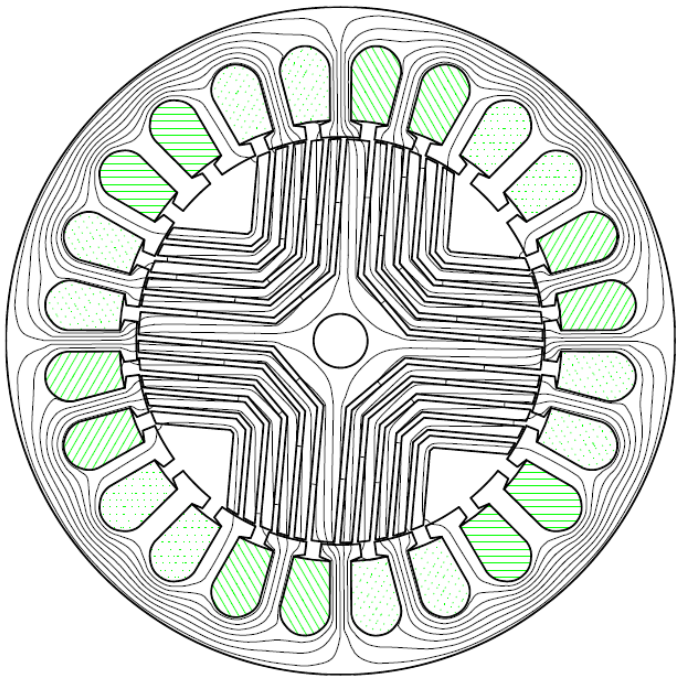

1342 QUADRATIC TRIANGULAR ELEMENTS, 2943 NODES
FLUX BETWEEN CURVES $4.26*10^{-4}$ Wb/m

Appendix E

Thermal Resistance of Stator Teeth [11]

This derivation has been done from the reference of [11] .

The thermal resistance is required to be integrated, as the area of the tooth is varying with the height. The figure shows a basic shape of a stator tooth.

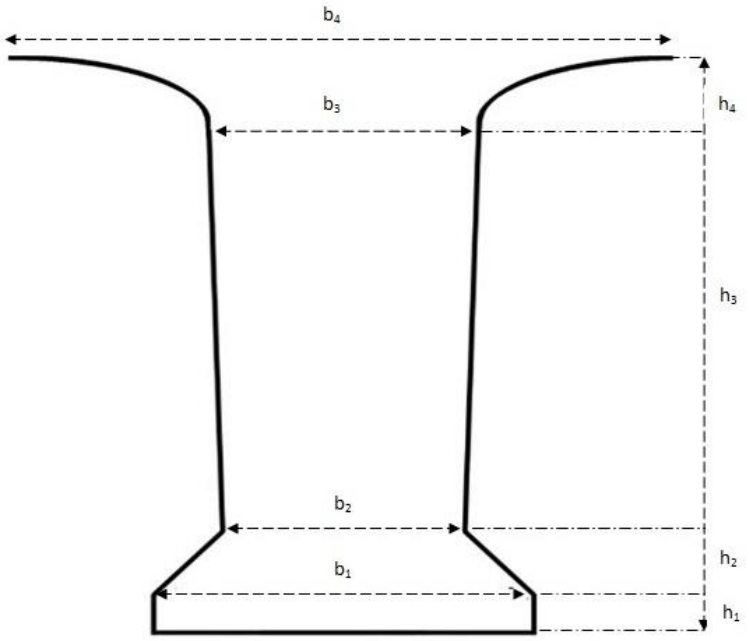

Figure C.1. Tooth geometry

$$R_t = \int_0^h \frac{1}{Q_s \, \lambda \, L \, b(h)} dh \qquad (C.1)$$

The tooth geometry can be divided in to four parts, D_1 to D_4. Now, the resistance is given by,

$$R_t = \int_0^h \frac{1}{2 \, Q_s \, \lambda \, L} \left[\int_0^{h1} \underbrace{\frac{dh}{b(h)}}_{D1} + \int_0^{h2} \underbrace{\frac{dh}{b(h)}}_{D2} + \int_0^{h3} \underbrace{\frac{dh}{b(h)}}_{D3} + \int_0^{h4} \underbrace{\frac{dh}{b(h)}}_{D4} \right] \qquad (C.2)$$

D_1

The width of tooth does not vary in radial direction.

$$\int_0^{h1} \frac{dh}{b(h)} = 2.\frac{h1}{b1} \qquad (C.3)$$

D_2 and D_3

In this part, the width changes with the height and hence the equation b(h) is required to be found before the integration.

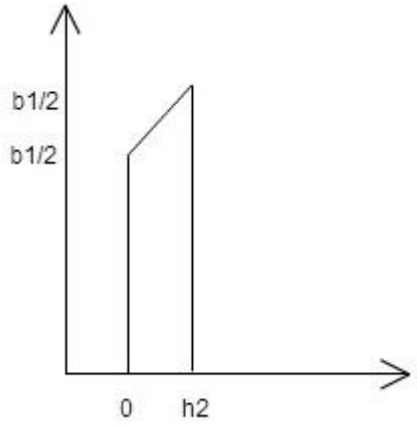

Figure C.2 Half of the tooth area D_2

$$b(h) = k.h + m \qquad (C.4)$$

$$k = \frac{\frac{b_2}{2} - \frac{b_1}{2}}{h_2} = \frac{b_2 - b_1}{2h_2} \rightarrow$$

$$m = \frac{b_1}{2} \qquad (C.5)$$

$$b(h) = \frac{b_2 - b_1}{2.h_2}.h + \frac{b_1}{2}$$

Put (C.5) in (C.3) gives,

$$\int_0^{h2} \frac{1}{b(h)} dh = \int_0^{h2} \frac{1}{\frac{b_2 - b_1}{2h_2} h + \frac{b_1 h_2}{2h_2}} dh$$

$$= 2h_2 \int_0^{h_2} \frac{1}{(b_2 - b_1)h + b_1 h_2}\, dh$$

$$= \left\{ \int \frac{dh}{ph+q} = \frac{1}{p} \int \frac{dh}{h + q/p} \right\}$$

$$= \left[h + q/p = u; dh = \frac{dh}{du} du = du \right]$$

$$= \left\{ (1/p). \int \frac{dh}{u} = \frac{1}{p} . \ln(h = q/p) \right\}$$

$$= \frac{2h_2}{b_2 - b_1} \ln(\frac{b_2}{b_1}) \qquad \text{(C.6)}$$

The same equation can be used for D_3 because they are almost identical in shape.

D_4

This part of the teeth is in the shape of an ellipse.

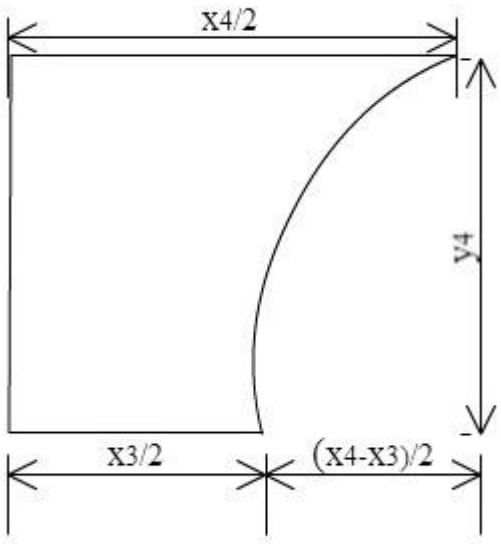

Figure C.3 Arc of the slot

$$1 = \frac{b^2}{p^2} + \frac{h^2}{q^2} \rightarrow$$

$$b = \sqrt{1 - \frac{h^2}{q^2}}$$

$$q = h_4$$

$$p = \frac{b_4 - b_3}{2}$$

which gives,

$$\int_0^{h4} \frac{1}{\frac{b_4}{2} - p\sqrt{1 - \frac{h^2}{p^2}}}\, dh$$

Substitute, $h = q.\sin\theta;\ dh = q.\cos\theta\, d\theta;\ h_4 = \pi/2$

$$\int_0^{\pi/2} \frac{q.\cos\theta}{\frac{b_4}{2} - p\sqrt{1 - \sin^2\theta}}\, d\theta \ \rightarrow \frac{q}{p}\int_0^{\pi/2} \frac{\cos\theta}{\underbrace{\frac{b_4}{2p}} - \cos\theta}\, d\theta \qquad ;\ \frac{b_4}{2p} = k$$

The general solution to the integral is given by,

$$\frac{q}{p}\left[-b - \frac{2K\tanh^{-1}\left((K+1).\tan b/2\right)}{\sqrt{1-K^2}}\right] \text{over the limit 0 to } \pi/2$$

The final simplified form is,

$$\frac{q}{p}\left[-\frac{\pi}{2} + \frac{2K}{\sqrt{1-K^2}}\tan^{-1}\left(\frac{1}{\sqrt{K-1}}\right)\right]$$